3. Articles I.: The effects of body mass

3.1. Foraging theory predicts predator–prey energy fluxes

a) Summary

1. In natural communities, populations are linked by feeding interactions that make up complex food webs. The stability of these complex networks is critically dependent on the distribution of energy fluxes across these feeding links.

2. In laboratory experiments with predatory beetles and spiders, we studied the allometric scaling (body-mass dependence) of metabolism and per capita consumption at the level of predator individuals and per link energy fluxes at the level of feeding links.

3. Despite clear power-law scaling of the metabolic and per capita consumption rates with predator body mass, the per link predation rates on individual prey followed hump-shaped relationships with the predator–prey body mass ratios. These results contrast with the current metabolic paradigm, and find better support in foraging theory.

4. This suggests that per link energy fluxes from prey populations to predator individuals peak at intermediate body mass ratios, and total energy fluxes from prey to predator populations decrease monotonically with predator and prey mass. Surprisingly, contrary to predictions of metabolic models, this suggests that for any prey species, the per link and total energy fluxes to its largest predators are smaller than those to predators of intermediate body size.

5. An integration of metabolic and foraging theory may enable a quantitative and predictive understanding of energy flux distributions in natural food webs.

b) Introduction

Natural ecosystems comprise a large number of species engaging in a vast number of predator–prey interactions of variable strength (Berlow et al. 2004; Wootton & Emmerson 2005). Two categories of interaction strength most commonly studied include (1) the magnitude of energy flowing from prey to predator, or predator consumption rates; and (2) the change in abundance of one species given a change in abundance of another, or the dynamic coupling of two species. Both measures provide insight into the stability of complex food webs (Brose et al. 2006b; Montoya, Pimm, & Sole 2006; Navarrete & Berlow 2006; Otto, Rall, & Brose 2007; Neutel et al. 2007; Rall et al. 2008). Thus a critical step for moving beyond descriptive, community-specific approaches in ecology is to uncover general principles that determine interaction strengths (Berlow et al. 2004; Brose et al. 2005b; Montoya et al. 2006). While not always directly related, high consumption rates (high energy fluxes) can establish the potential for strong dynamic coupling between two species (Brose et al. 2005b; Bascompte, Melián, & Sala 2005). Here we focus on general principles that determine energy fluxes, because recent allometric models based on metabolic scaling theory (Brown et al. 2004) have proposed that predator consumption rates follow a power-law increase with predator body mass (Yodzis & Innes 1992; Emmerson & Raffaelli 2004; Reuman & Cohen 2005; Wootton & Emmerson 2005). The elegant simplicity and empirical tractability of this theory has led to its recent widespread application in theoretical studies (McCann et al. 1998; Emmerson & Raffaelli 2004; Williams & Martinez 2004a; Brose et al. 2006b).

By defining physiological constraints, metabolic theory predicts the per capita (per individual) and total consumption rates necessary to sustain a population. However, being based only on predator body masses, this approach cannot distinguish the energy fluxes among the individual feeding links of generalist predators (hereafter, per link fluxes). It thus predicts per link fluxes by distributing per capita consumption rates equally across the feeding links. In contrast, foraging theory uses traits of the prey species, such as average body masses (where the average is an evolutionarily stable mean over the individuals of a population), to predict how behavioural aspects of predator–prey interactions determine the relative strength of these feeding links while ignoring the overall energy flux at the level of predator individuals. Here we propose a framework that integrates metabolic theory at the levels of predator individuals (per capita) with foraging theory at the level of feeding interactions (per link). Our focus on predator–prey energy fluxes complements recent analyses of how allometric foraging models predict food-web topology (Beckerman, Petchey, & Warren 2006). We first introduce the models, then test their predictions using laboratory data on metabolism and consumption of arthropods. Macroecological abundance-mass relationships scale-up

these predictions to natural communities with variance in predator and prey abundance.

c) Models

Per capita metabolism and consumption

At the level of individuals, metabolic theory predicts that the metabolic rates of species i, I_i, [J s^{-1}] scale with body mass, M_i (g) as:

$$I_i = I_0 M_i^a \tag{3.1.1}$$

where I_0 and a are constants (Brown et al. 2004). Moreover, it predicts that per capita consumption rates of consumer individuals of species i, C_i [J s^{-1}], follow a similar mass-dependence to the metabolic rates:

$$C_i = C_0 M_i^b \tag{3.1.2}$$

where C_0 and b are constants (Carbone, Teacher, & Rowcliffe 2007).

Per link consumption

Direct application of this per capita relationship (equation 3.1.2) to individual feeding interactions between predator i and prey j yield per link consumption rates, K_{ij} [J s^{-1}]:

$$K_i = K_0 M_i^b \tag{3.1.3}$$

where K_0 is a constant and

$$C_i = \sum_j K_{ij}$$

(Yodzis & Innes 1992; Brown et al. 2004). This 'metabolic model' predicts energy fluxes through individual links by distributing the predator's per capita consumption rate equally across its feeding links.

In contrast, foraging theory suggests that per link predation rates P_{ij} [ind s^{-1}] (the number of individuals of prey j consumed per individual of predator i) follow a hump-shaped relationship with predator-prey body-mass ratios $R_{ij} = M_i M_j^{-1}$:

$$P_{ij} = P_{max}\left[\frac{R_{ij}}{R_{max}} e^{1-\frac{R_{ij}}{R_{max}}}\right]^{\gamma} \tag{3.1.4}$$

where P_{max} [ind s^{-1}] is the maximum predation rate, R_{max} is the body-mass ratio at which this

maximum is achieved, and γ is a scaling constant (Wilson 1975; Persson et al. 1998; Wahlström et al. 2000; Byström et al. 2003; Aljetlawi, Sparrevik, & Leonardsson 2004; Finstad, Ugedal, & Berg 2006). This phenomenological foraging model describes (1) predation rates increasing with body mass ratios when predators are small relative to their prey ($R_{ij} < R_{max}$), which is explained by an increasing ability of the predator to subdue and handle prey; and (2) predation rates decreasing with body mass ratios when predators are large relative to their prey ($R_{ij} > R_{max}$), which results from a decreasing detectability and catchability of smaller prey (Persson et al. 1998; Aljetlawi et al. 2004).

Macroecological energy fluxes

The metabolic model (equation 3.1.3) and the foraging model (equation 3.1.4) predict laboratory energy fluxes at a fixed abundance, N'_j [ind]. This implies similar laboratory encounter rates for each prey: E'_{ij} [ind s^{-1}] = $E'_0 N'_j$, where E'_0 and N'_j are constants that are independent of body mass. In natural communities, however, field encounter rates, E'_{ij} [ind s^{-1}] = $E'_0 N'_j$ depend on field prey abundance, N_j [ind] (Emmerson, Montoya, & Woodward 2005) that scales with body mass as:

$$N_j = N_0 M_j^{-c} \tag{3.1.5}$$

where N_0 and c are macroecological constants and often $c \approx 0.75$ (Brown et al. 2004; Meehan 2006a). Synthesizing either the metabolic model or the foraging model with this macroecological abundance–mass relationship scales up predictions from laboratory to field conditions. The per capita energy flux, F_{ij} [J s–1], through the link from prey population $_j$ to an individual of predator population i, can be derived under the metabolic model by normalizing the per link consumption rates (equation 3.1.3) by the laboratory encounter rates, E'_{ij}, and multiplying them with field encounter rates, E_{ij}:

$$F_{ij} = K_{ij} E'^{-1}_{ij} E_{ij} = K_{ij} E'^{-1}_0 N'^{-1}_j E_0 N_j = E'^{-1}_0 E_0 N_0 K_0 N'^{-1}_j M_i^b M_j^{-1} \tag{3.1.6a}$$

This approach distributes per capita consumption rates across feeding links using encounter rates that apply to averages over individuals within populations, while ignoring differences among individuals. Under the foraging model (equation 3.1.4), F_{ij} [J s^{-1}] is equal to predation rates, P_{ij} [ind s-1] divided by the laboratory encounter rate, E'_{ij}, and multiplied by the field encounter rate, E_{ij}, and prey energy content [the product of prey mass, M_j [g ind^{-1}] and the energy content per wet mass ε [J g^{-1}] :

$$F_{ij} = P_{ij} E'^{-1}_{ij} E_{ij} \varepsilon M_j = P_{ij} E'^{-1}_0 N'^{-1}_j E_0 N_j \varepsilon M_j = E'^{-1}_0 N'^{-1}_j E_0 N_0 \varepsilon P_{ij} M_j^{1-c} \tag{3.1.6b}$$

The total energy flux from prey population j to predator population i, T_{ij} [J s^{-1}], is defined as the product of the per capita energy flux (equation 3.1.6a or 3.1.6b) and predator abundance

$N_i (N_i = N_0 M_i^{-c})$, which yields:

$$T_{ij} = E'^{-1}_0 E_0 K_0 N_0^2 N'^{-1}_j M_i^{b-c} M_j^{-c} \quad (3.1.7a)$$

$$T_{ij} = E'^{-1}_0 N'^{-1}_j E_0 N_0^2 \varepsilon P_{ij} M_i^{-c} M_j^{1-c} \quad (3.1.7b)$$

under the metabolic (equation 3.1.7a) and foraging (equation 3.1.7b) model, respectively.

d) Methods

We used ground-dwelling beetles and spiders to test these model predictions in laboratory experiments. Pitfall trapping yielded 16 carabid and staphylinid beetle species (Abax ovalis, *Abax parallelepipedus*, *Calathus melanocephalus*, *Calathus piceus*, *Carabus auratus*, *Harpalus affinis*, *Nebria brevicollis*, *Notiophilus biguttatus*, *Notiophilus laticollis*, *Ocypus olens*, *Philonthus fuscipennis*, *Platynus dorsalis*, *Poecilus versicolor*, *Pseudophonus rufipes*, *Pterostichus melanarius*, *Pterostichus oblongopunctatus*) and 10 lycosid, pisaurid and salticid spider species (*Alopecosa* sp. juv. I, *Alopecosa* sp. juv. II, *Alopecosa cuneata*, *Pardosa lugubris*, *Pardosa palustris*, *Pirata piraticus*, *Pirata latitans*, *Pisaura mirabilis*, *Salticus scenicus*, *Trochosa terricola*; for authorities see Brohmer & Schaefer 2006). The juveniles of *Alopecosa* sp. were considered as trophic species as they vary from adults in their prey spectrum. We used only adult females of the other spider species. The species chosen are common epigeic predators in central Europe.

All experiments were carried out under controlled laboratory conditions (12 h light per day, 15°C). We measured the basal metabolic rates of six individuals of each species with an automated electrolytic microrespirometer (Scheu 1992). We converted the measured O_2 fluxes (ml O_2 s^{-1}) per spider individual into energetic equivalents (J s^{-1}) by assuming that 1 ml O_2 equals 20.1 J. Prior to the consumption experiments, the predator species were fed and then starved for 5 days. All individuals were weighed before and after the experiments on a precision scale. We used the average of these weights throughout all analyses. We used collembolans (*Heteromurus nitidus*) and crickets (*Gryllus sigillatus*) as prey for the spiders, and fruit flies (*Drosophila hydei*) and fly larvae (*Lucilia caesar*) as prey for the beetles, which yielded a total of 32 and 20 predator-prey interactions for beetles and spiders, respectively. We studied predation by placing one predator individual in each arena (0.2 × 0.2 m), in which 2.35 g dry moss (*Polytrichum formosum*) was evenly dispersed as habitat structure. The moss was dried for 4 days at 60°C to exclude other animals, and was moisturised prior to the experiments. In each experimental replicate, one predator individual and 30 individuals of one prey species (initial prey density N_i) were placed in an arena, and we counted the number of prey that remained after 24 h (final prey density N_e). We used eight replicates per predator-prey combination, and calculated the energy fluxes for each replicate (K_{ij} in equation 3.1.3) by

multiplying the number of prey individuals consumed ($N_c = N_i - N_e$) by the average weight of the prey individuals (g) and the energy content per mg prey wet mass (7 J g^{-1}) (Peters 1983). The use of this general energy content per mg wet mass ignores taxon-specific variation in energy density due to difference in stoichiometry. Given that most of the variation in predator–prey body mass ratios was caused by variance in predator body masses, this generalization appears to cause a relatively small error in energy contents. The predation rates (P_{ij} in Eqn. 3.1.4) equalled the number of prey individuals consumed per individual predator. Control treatments without predators exhibited similar prey densities at the beginning and end of the experiment, suggesting that any decline in prey density in predator enclosures was due to consumption rather than natural mortality. The per capita consumption rates of the predator species (C_i in Eqn. 3.1.2) were calculated under the assumptions that the predators encounter and attack their prey by chance, and we averaged the independently measured per link consumption rates of the two prey populations [$j = 1, 2$; $C_i = (K_{i1} + K_{i2})/2$ or $C_i = K_{ij}$ if only j is consumed].

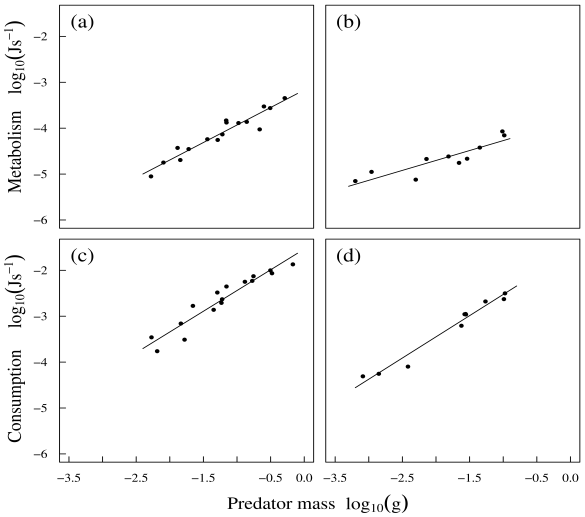

Figure 3.1.1: Laboratory measurements at the species level: metabolism, **(a)** beetles; **(b)** spiders) [$\log_{10}$ (J s^{-1})] and per capita consumption, **(c)** beetles; **(d)** spiders [$\log_{10}$ (J s^{-1})] depending on predator body mass ($\log_{10}$ g). Fitted model parameters (± SE). **(a)** Equation 1: $a = 0.76 \pm 0.06$; $\log_{10} I_0 = -3.17 \pm 0.09$; $r^2 = 0.91$; $P < 0.0001$; $n = 16$; **(b)** equation 1: $a = 0{\cdot}43 \pm 0{\cdot}07$; $\log_{10} I_0 = -3{\cdot}84 \pm 0{\cdot}16$; $r^2 = 0.8$; $P < 0{\cdot}001$; $n = 10$; **(c)** equation 2: $b = 0.9 \pm 0.08$; $\log_{10} C_0 = -1.54 \pm 0.1$; $r^2 = 0{\cdot}91$; $P < 0{\cdot}0001$; $n = 16$; **(d)** equation 2: $b = 0.92 \pm 0.06$; $\log_{10} C_0 = -1.6 \pm 0.11$; $r^2 = 0.97$; $P < 0.001$; $n = 10$. Predator individuals were the same in upper **(a,b)** and lower **(c,d)** panels, but their body masses were slightly heavier in the lower panels because we averaged their masses before and after the feeding experiments.

We calculated the averages of the metabolic rate, the per capita consumption rate and the body mass for each predator species, and the averages of the predation rate, per link consumption rate and body mass ratio for each predator–prey interaction. The relationships between (1) average metabolic rate and average predator body mass; (2) average per capita consumption rate and average predator body mass; (3) average per link consumption rate and average predator body mass; and (4) average predation rate and average predator–prey body mass ratio were all analysed by nonlinear least-squares regressions.

e) Results

Per capita metabolism and consumption

The metabolic rates exhibited a power-law increase with the average body mass of the species, but the exponent of the relationship was higher for beetles (a = 0·76 ± 0·07; mean ± SE, Fig. 3.1.1a) than for spiders (a = 0·43 ± 0·07; Fig. 3.1.1b). The per capita consumption rates also followed a power-law relationship with the average body mass, but the slopes were steeper (Fig. 3.1.1c,d).

Per link consumption

At the level of feeding links, the metabolic model (Eqn. 3.1.3) gave a poor fit to the per link consumption rate data for beetles (Fig. 3.1.2a, r^2 = 0·39) and spiders (Fig. 3.1.2b, r^2 = 0·36). Interestingly, the per link consumption rates of large predators were higher than predicted by the metabolic model when they consumed the larger of the two prey species (fly larvae for beetles; crickets for spiders; Fig. 3.1.2a,b), and were lower than predicted when they consumed the smaller of the two prey species (fruit flies for beetles; collembolans for spiders; Fig. 3.1.2a,b). The hump-shaped foraging model (Eqn. 3.1.4) explained a much higher fraction of the variation in predation rates of beetles (Fig. 3.1.2c, r^2 = 0·60) and spiders (Fig. 3.1.2d, r^2 = 0·78). The maximum predation rates were reached at intermediate body mass ratios of R_{max} = 38·1 ± 6·2 and R_{max} = 103·1 ± 14·5 (mean ± SE) for beetles and spiders, respectively. Observations during the experiments suggest that predation was limited by the relatively long time needed to subdue and handle the prey at low body mass ratios. At high body mass ratios, predation was limited by the high escape efficiencies of prey species due to fast reaction times and their use of small refuges in the moss vegetation.

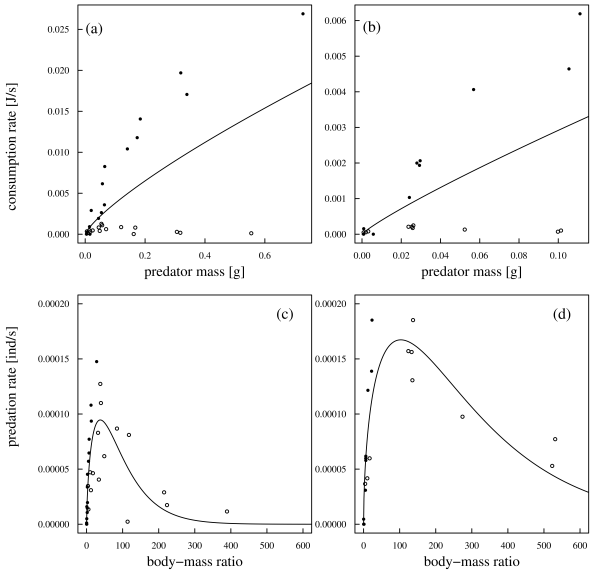

Figure 3.1.2: Laboratory measurements at the level of feeding links: per link consumption rates [J s^{-1}] depending on predator body mass (g), **(a)** beetles; **(b)** spiders and predation rates (ind s^{-1}) depending on predator–prey body mass ratios, **(c)** beetles; **(d)** spiders. Fitted model parameters (± SE): metabolic model (equation 3) for **(a)** beetles (b = 0.78 ± 0.22; K_0 = 0.02 ± 0.01; r^2 = 0.39; n = 32); **(b)** spiders (b = 0.87 ± 0.42; K_0 = 0.02 ± 0.02; r^2 = 0.36; n = 20); foraging model (equation 4) for **(c)** beetles (P_{max} = 9.46 10^{-5} ± 9.59 10^{-6}; R_{max} = 38.1 ± 6.17; α = 0.68 ± 0.16; r^2 = 0.6; n = 32); **(d)** spiders (P_{max} = 1.67 10^{-4} ± 1.45 10^{-5}; R_{max} = 103.1 ± 14.47; α = 0.54 ± 0·1; r^2 = 0.78; n = 20). Symbols indicate large prey (closed circles) and small prey (open circles).

Macroecological energy fluxes

Synthesizing macroecological abundance–mass relationships with the metabolic model (Eqn. 3.1.6a) and the foraging model (Eqn. 3.1.6b) yields predictions on per capita energy fluxes from a prey population to a predator individual with respect to predator and prey mass (Fig. 3.1.3a,b). Due to assumed constants (see Fig. 3.1.3 legend) the predicted fluxes should be interpreted only qualitatively. The predictions are based on the measured laboratory per link consumption and predation rates for beetles (Fig. 3.1.2a,c), but calculations based on the results for spiders yield qualitatively identical predictions (results not shown). The metabolic model predicts a continuous increase in per capita energy fluxes with increasing predator mass and decreasing prey mass (Fig. 3.1.3a). In contrast, the foraging model predicts a hump-shaped relationship between per capita energy fluxes and predator masses, where the hump increases with prey mass (Fig. 3.1.3b).

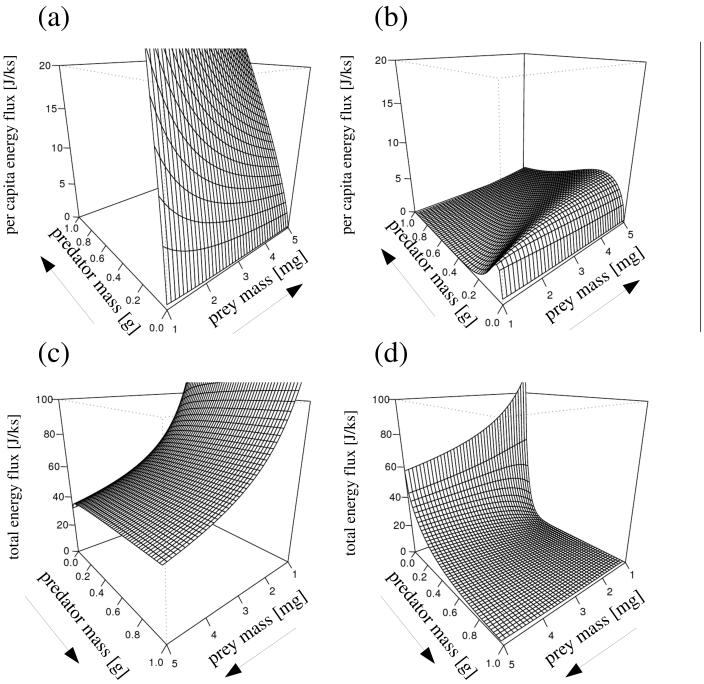

Figure 3.1.3: Per capita (**a,b**: from a prey population to a predator individual) and total (**c,d**: from a prey population to a predator population) energy flux as predicted by the synthetic models combining macroecological abundance–mass relationships with the metabolic model: **(a)** equation 3.1.6a; **(c)** equation 3.1.7a; or the foraging model: **(b)** equation 3.1.6b; **(d)** equation 3.1.7b, depending on predator **(g)** and prey body mass (mg). Calculations are based on per link consumption rates (**a,c**, see Fig. 3.1.2a) or predation rates (**b,d**, see Fig. 3.1.2c) and assumed constants: $E'_0 = E_0 = N_0 = 1$; $N'_0 = 30$; $\varepsilon = 7$; $c = 0{\cdot}75$. Thus energy flux values should be interpreted only qualitatively. ks = 10^3 s.

Multiplying per capita energy fluxes (Fig. 3.1.3a,b) with predator abundances yields total energy fluxes between prey and predator populations. The metabolic model (Eqn. 3.1.7a) predicts that the total energy fluxes increase with increasing predator mass and decreasing prey mass (Fig. 3.1.3c). The highest fluxes should thus occur between the smallest prey and the largest predators. In contrast, the foraging model (Eqn. 3.1.7b) predicts that the highest fluxes should occur between the smallest predators and the smallest prey species (Fig. 3.1.3d).

f) Discussion

At the species level, we found a three-quarter power-law scaling of the metabolic rates with body masses for beetles, which corroborates metabolic theory (Brown et al. 2004). Consistent with prior findings (Foelix 1996), the respiration rates of spiders were lower than those of beetles. Surprisingly, however, we found a much weaker increase in spider metabolism with body mass than predicted by the metabolic theory. Potential explanations for this discrepancy include that (1) the relative contribution of metabolically active tissue to total body mass of small spiders might exceed that in large spiders due to different rates of excretion-storage in their skins (Foelix 1996); and (2) spider metabolism might be limited by factors other than the efficiency of their physiological transport networks (Meer 2006). Corroborating metabolic theory, our data illustrate that the per capita consumption rates of both predator groups follow a power-law increase with body mass and exceed the metabolic loss, thus enabling the persistence of the predators.

While each predator's metabolic rate and total consumption were well predicted by power-law functions of predator body mass, the energy fluxes along individual predator–prey links were not. When predator–prey body mass ratios exceeded a threshold (R_{max}), the energy fluxes were limited by a decreasing success rate of the predator attacks due to a higher escape efficiency of the prey. Without the constraints posed by limited attack success, the metabolic model predicts a much stronger increase in energy flux with prey abundance. Interestingly, the two predator groups in our study represent profoundly different feeding strategies: spiders are mainly day-active, optically oriented predators, whereas beetles are mainly nocturnal, tactile and olfactory predators. However, the hump-shaped relationship between predation rates and body mass ratios found for both predator groups was well predicted by a foraging model, which is consistent with prior studies in aquatic ecosystems (Wahlström et al. 2000; Byström et al. 2003; Aljetlawi et al. 2004; Finstad et al. 2006). While these studies addressed predation rates in size-structured predator–prey interactions with respect to the body masses of individuals, we studied predation rates as a function of the average masses of predator and prey populations. The foraging model used here and in related studies (Wahlström et al. 2000; Aljetlawi et al. 2004) is phenomenological, and the hump-shaped relationship is fit equally well by two power-laws ($P_{ij} \approx R^{\varphi}$ if $R \leq R_{max}$; $P_{ij} \approx R^{-\eta}$ if $R > R_{max}$). However, independent of the choice of model, the broad generality of this hump-shaped relationship across ecosystem types and predator groups suggests that metabolic energy-flux models (Peters 1983; Emmerson & Raffaelli 2004; Reuman & Cohen 2005) that do not account for this relationship may seriously overestimate per capita energy fluxes between large predators and small prey. Moreover, the hump-shaped relationship between predation rates and predator-prey body mass ratios contrasts classic population dynamic models using power-law per link consumption rates (Yodzis & Innes 1992), whereas it corroborates recent approaches with unimodal

predation rates (Loeuille & Loreau 2005; Weitz & Levin 2006). These patterns suggest that, all else being equal, the dynamic coupling between large predators and small prey may generally be weaker than predicted by a simple metabolic model. As general principles that govern energy flux may be more tractable than those that determine the population dynamics of species interaction strengths, it is critical to explore more thoroughly how and when consumer foraging patterns can predict the dynamic consequences of a change in consumer abundance (Schmitz 2007).

Some caveats should be mentioned. First, all laboratory experiments were carried out with simple predator–prey pairs, not accounting for potentially more complex feeding behaviour of predators when multiple prey species or multiple predator individuals coexist (e.g. prey switching or interference competition). Second, our estimates of field energy fluxes assume that consumption rates increase linearly with prey abundances (encounter rates) (Emmerson & Raffaelli 2004; Neutel et al. 2007). Where handling and satiation lead to consumption saturation at high prey densities, we anticipate that energy fluxes should always saturate, rather than increase monotonically as prey body mass decreases (and thus prey abundance increases). Third, encounter rates may be influenced by body mass-related species traits such as the search area of the predator and the movement velocity of predator and prey (Aljetlawi et al. 2004). While these caveats may change some quantitative aspects of the model predictions (e.g. the continuous increase in total energy flux with decreasing prey body mass), qualitative differences among predictions of the metabolic and foraging models should be robust. Most importantly, this includes (1) the power-law (metabolic model) vs. hump-shaped (foraging model) relationship between per capita energy flux and predator body mass; and (2) the increase (metabolic model) vs. decrease (foraging model) in total energy flux with predator body mass. Future extensions of our approach will address how more complex foraging models that account for the caveats listed above may change the quantitative predictions of the models.

While metabolic theory accurately predicts physiological processes at the level of individuals (per capita metabolic demand and consumption) (Brown et al. 2004), it failed to accurately predict per link energy fluxes at high predator–prey body mass ratios. At these high ratios, energy fluxes were not driven by the predators' metabolic demand as assumed by metabolic theory. Instead, they depended primarily on behavioural aspects of the interaction, such as the prey's escape efficiency that increased with predator-prey body mass ratios (for $R > R_{max}$). Rooted in behavioural models of foraging theory, the hump-shaped foraging model successfully predicted the energy fluxes in the present study. Thus reconciling these two bodies of theory that successfully predict patterns at the level of individuals (metabolic theory) and links (foraging theory) will be an important step towards quantitative community ecology that predicts energy fluxes and abundances.

Interestingly, the predator–prey body mass ratios that characterize the maximum predation rates in our experiments are consistent with the average predator–prey body mass ratios found in natural food webs (Brose et al. 2006a). Consistent with prior studies (Wilson 1975; Wahlström et al. 2000; Byström et al. 2003; Aljetlawi et al. 2004; Finstad et al. 2006) our results suggest that predators may efficiently exploit prey that fall within a specific size range. Such a contiguous feeding range is also consistent with successful theoretical concepts of adaptive (Uchida, Drossel, & Brose 2007) and static food web topology (Williams & Martinez 2000; Loeuille & Loreau 2005; Stouffer, Camacho, & Amaral 2006). Moreover, the foraging model predicts energy fluxes through individual feeding links, which offers a new perspective on the distribution of interaction strengths within food webs that ultimately drive network stability (Emmerson & Raffaelli 2004; Brose et al. 2006b; Montoya et al. 2006; Neutel et al. 2007). Specifically, our results suggest that the dominant per capita energy fluxes within a food web that are critically important for its stability (Bascompte & Melian 2005; Otto et al. 2007; Neutel et al. 2007) occur between predator–prey pairs of intermediate body mass ratios (Fig. 3b). If our results generalize to other predator groups and ecosystem types, this approach allows predicting quantitative energy fluxes in natural food webs (Bersier, Banasek-Richter, & Cattin 2002). Ultimately, we anticipate that this will enable a quantitative understanding of interaction strengths, energy fluxes and the stability of complex natural food webs.

3.2. Allometric functional response model: body masses constrain interaction strengths

a) Summary

1. Functional responses quantify the per capita consumption rates of predators depending on prey density. The parameters of these nonlinear interaction strength models were recently used as successful proxies for predicting population dynamics, food-web topology and stability.

2. This study addressed systematic effects of predator and prey body masses on the functional response parameters handling time, instantaneous search coefficient (attack coefficient) and a scaling exponent converting type II into type III functional responses. To fully explore the possible combinations of predator and prey body masses, we studied the functional responses of 13 predator species (ground beetles and wolf spiders) on one small and one large prey resulting in 26 functional responses.

3. We found (i) a power-law decrease of handling time with predator mass with an exponent of -0.94; (ii) an increase of handling time with prey mass (power-law with an exponent of 0.83, but only three prey sizes were included); (iii) a hump-shaped relationship between instantaneous search coefficients and predator–prey body-mass ratios; and (iv) low scaling exponents for low predator–prey body mass ratios in contrast to high scaling exponents for high predator–prey body-mass ratios.

4. These scaling relationships suggest that nonlinear interaction strengths can be predicted by knowledge of predator and prey body masses. Our results imply that predators of intermediate size impose stronger per capita top-down interaction strengths on a prey than smaller or larger predators. Moreover, the stability of population and food-web dynamics should increase with increasing body-mass ratios in consequence of increases in the scaling exponents.

5. Integrating these scaling relationships into population models will allow predicting energy fluxes, food-web structures and the distribution of interaction strengths across food web links based on knowledge of the species' body masses.

b) Introduction

Understanding constraints on species' interaction strengths is critically important for predicting population dynamics, food-web stability and ecosystem functions such as

biological control (Berlow et al. 2004; Montoya et al. 2006; Wootton & Emmerson 2005). Empirical and theoretical evidence suggests that predator and prey body masses are among the most important of these constraints (Emmerson & Raffaelli 2004; Wootton & Emmerson 2005; Woodward et al. 2005; Berlow, Brose, & Martinez 2008; Berlow et al. 2009). Conceptually, these nonlinear interaction strengths are described by the magnitude and shape of functional responses that quantify per capita consumption rates of predators depending on prey abundance. One generalized functional response model is based on Holling's disk equation (Holling 1959b):

$$F_{(N)} = \frac{bN^{q+1}}{1 + bT_h N^{q+1}} \qquad (3.2.1)$$

where F is the per capita consumption rate, N is prey abundance, T_h is the handling time needed to kill, ingest and digest a resource individual, b is a search coefficient that describes the increase in the instantaneous search rate, a, with resource abundance, N:

$$a = bN^{q} \qquad (3.2.2)$$

where q is a scaling exponent that converts type II into type III functional responses (Williams & Martinez 2004a; Rall et al. 2008). The hill exponent, h, used in some prior studies (Real 1977) is equivalent to q ($h = q + 1$).

Functional responses can be linear (type I, $T_h = 0$, increase up to a threshold abundance), hyperbolic (type II, $T_h > 0$, $q = 0$) or sigmoid (type III, $T_h > 0$, $q > 0$). While many early studies focused on type I and type II functional responses and ignored the scaling exponent, type III functional responses with scaling exponents larger than zero could occur more frequently than previously anticipated (Sarnelle & Wilson 2008). Under hyperbolic type II functional responses predation risks for prey individuals decrease with prey abundance causing inverse density-dependent prey mortality, which can lead to unstable boom-burst population dynamics (Oaten & Murdoch 1975a; Hassell 1978). In contrast, increasing predation risks under sigmoid functional responses can yield an effective per capita top-down control that often prevents such unstable dynamics (Rall et al. 2008; Gentleman & Neuheimer 2008). Slight differences in functional response parameters can thus have drastic consequences for population and food-web stability in natural ecosystems (Oaten & Murdoch 1975a; Williams & Martinez 2004a; Fussmann & Blasius 2005; Brose et al. 2006b; Rall et al. 2008).

Allometric scaling theories provide a conceptual framework how body masses could determine foraging interactions (Peters 1983; Brown et al. 2004). The maximum consumption rates realized at infinite prey densities are proportional to the inverse of handling time and independent of the success of the attacks (Yodzis & Innes 1992; Koen-Alonso 2007).

Consequently, the 3/4 power-law scaling of maximum consumption with predator body mass (Peters 1983; Carbone et al. 1999) suggests that handling time should follow a negative ¾ power-law with predator body mass. This trend is qualitatively supported, though studies reported linear (Hassel, Lawton, & Beddington 1976; Spitze 1985), power-law or exponential relationships (Thompson 1975; Hassel et al. 1976; Aljetlawi et al. 2004; Jeschke & Tollrian 2005).

The characteristic components of search rates include the reactive distance between predator and prey (i.e. the distance between predator and prey individuals at which a predator individual responds to the presence of the prey) and the capture success. While the reactive distance increases with the body masses of the predators (i.e. large predators have a larger visual range than small predators), the capture success decreases with predator mass above an optimum body mass ratio (Aljetlawi et al. 2004; Brose et al. 2008). A further explanation for the low capture success is that the predator's motivation to capture small prey of limited energy content is low (Petchey et al. 2008). Together, these patterns in reactive distances and capture success may explain the hump-shaped relationships between search rates and predator-prey body-mass ratios with a maximum search rate at intermediate (optimum) body-mass ratios documented in prior studies (Hassel et al. 1976; Wahlström et al. 2000; Aljetlawi et al. 2004; Vonesh & Bolker 2005; Brose et al. 2008). However, these studies were either restricted to search rates of single predator–prey interactions (with variance in individual size) or studied multiple predator-prey search rates at a single, constant prey density. Thus, none of these prior studies has addressed body-size constraints on functional responses across species.

In this study, we quantified systematic effects of predator and prey masses on functional response parameters (handling time, search coefficient and scaling exponent) across different predator–prey interactions. While more complex functional response models accounting for digesting time and interference behaviour exist (Skalski & Gilliam 2001; Jeschke et al. 2002; Schenk, Bersier, & Bacher 2005; Kratina et al. 2009), testing for their body-size dependence was left for subsequent studies. Instead, the allometric functional response model addressed here provide an empirical basis for an understanding of body-size constraints on interaction strengths, food-web topology (Petchey et al. 2008) and dynamics (Brose et al. 2006b; Otto et al. 2007; Rall et al. 2008; Brose 2008).

c) Methods

The predators of our experiment were carabid beetles (*Abax parallelepipedus*, *Carabus nemoralis*, *Pterostichus melanarius*, *Pterostichus oblongopunctatus*, *Harpalus rufipes*, *Calathus fuscipes*, *Calathus melanocephalus*, *Anchomenus dorsalis* and *Poecilus versicolor*; Carabidae: Coleoptera) and wolf spiders (*Trochosa terricola*, *Pardosa lugubris*; Aranea:

Lycosidae) sampled in pitfall traps. The juvenile weight classes of 1, 3 and 10 mg of Trochosa were considered as trophic species as they vary in consumption rates and preferences for the different prey species (Rickers & Scheu 2005; Brose et al. 2008). We used *Alphitobius diaperinus* larvae (Coleptera; Tenebrionidae; hereafter: *Alphitobius*), flightless adults of *Drosophila hydei* (Diptera; Drosophilidae, hereafter: *Drosophila*) and *Heteromurus nitidus* (Collembola; Entomobryidae, hereafter: *Heteromurus*) as prey.

Functional Response Experiments

To explore fully possible combinations in predator and prey body masses, we studied the functional response of each predator on one small and one large prey. For the beetles, we used flightless *Drosophila* as small prey and *Alphitobius* as large prey. For the spiders, we used *Heteromurus* as small prey and flightless Drosophila as large prey. Each experimental unit included one predator individual and prey at different initial densities that were varied between low densities (1, 3, 5, 10, 20, 30 prey individuals per experimental arena) and higher prey densities that were adjusted to each specific predator–prey combination to reach saturation in the predators per capita consumption rate (e.g. 120 individuals of *Drosophila* for the small predator *Anchomenus dorsalis* and 4000 individuals of *Drosophila* for the large predator *Carabus nemoralis*). Six replicates per prey density were established. The predator individuals were kept separate in plastic jars dispersed with water and were deprived of food for 1 week prior to the start of the experiments. The experiments were performed in Perspex® (Degussa AG, Darmstadt, Germany) arenas (20 x 20 x 10 cm) covered with lids that had holes to allow gas exchange. The ground was covered with moist plaster (200 g dry weight) to provide constant moisture during the experiments. Habitat structure in the arenas was provided by moss (*Polytrichum formosum*, 2.43 g dry weight) that was first dried for several days at 40°C to exclude other animals and then re-moisturised. The experiment was run for 24 h with a day / night rhythm of 12 / 12 h dark / light and temperature of 15°C. Initial and final prey densities were used to calculate the number of prey eaten. Control experiments without predators showed that prey mortality or escape did not influence our experiments. The predators were weighed before and after the experiment to calculate the mean body mass of each predator and the body-mass ratio of each predator-prey pair (Table 3.2.1).

Statistical Analyses

In the present study, the prey densities changed during the experimental period with each consumption event. To account for this prey depletion during the experiments, we used a generalized model of Rogers's random predator equation (Rogers 1972; Juliano 2001):

$$N_e = N_0(1-\exp(bN_0^q(T_h N_e - T))) \qquad (3.2.3),$$

where N_e is the number of prey eaten, N_0 is the initial prey density, b is the search coefficient (search rate $a = bN_0^q$), Th is the handling time, T is the experimental duration time and q is the scaling exponent. We fitted equation (3.2.3) to the experimental data using Newton's method in **SAS** 9.1 (Juliano 2001) to obtain parameter estimates. We prevented (i) negative scaling exponents (i.e. decreases in search rates with prey density) and (ii) negative handling times. Subsequently, we tested for effects of predator and prey masses on handling times, search coefficients and hill exponents. We used linear least-squares regressions to test for relationships between $\log_{10}$ handling time vs. $\log_{10}$ predator mass and $\log_{10}$ prey mass:

$$\log_{10} T_h = p \log_{10} M_P + n \log_{10} M_N + \log_{10} T_{h(0)} \qquad (3.2.4)$$

with T_h as handling time, M_P as predator mass, M_N as prey mass, and p, n, $T_{h(0)}$ as constants. Hump-shaped relationships between $\log_{10}$-transformed search-coefficients, b, and predator–prey body-mass ratios, R, were tested by fitting the following size–search-coefficient curve in **R** (R-Project 2.8.1, free statistic software; The R Foundation for Statistical Computing, Vienna, Austria):

$$\log_{10}(b_{(R)}+1) = A \frac{\exp(\varepsilon(\Phi - \log_{10}(R+1)))}{1+\exp(\beta\varepsilon(\Phi - \log_{10}(R+1)))} \qquad (3.2.5)$$

where A is a constant, Φ represents the body mass ratio at which 50% of the maximum search coefficient is reached, e is the rate of change in search with size controlling the steepness of the curve, R is the body-mass ratio and b determines the asymmetry of the curve (Vonesh & Bolker 2005). To find the optimum body mass ratio, R_0, where the maximum search coefficient is reached, the first derivative of equation (3.2.4) has to be set equal to zero and solved for R_0, resulting in the following equation (Vonesh & Bolker 2005):

$$\log_{10}(R_0+1) = \frac{\Phi + \log_{10}(\beta - 1)}{\varepsilon\beta} \qquad (3.2.6)$$

The solution of equation (3.2.6) can be inserted in equation (3.2.5) to calculate the maximum search coefficient, $b_{max}(R_0)$.We tested for significant differences in scaling exponents, q, between predator-prey pairs using an ANOVA. Subsequently, we employed two contrast analyses (one for spiders and one for beetles) to test our hypothesis that the scaling exponent is higher for high predator-prey body-mass ratios (small prey) than for low ratios (large prey).

d) Results

Across the 26 functional responses of the present study (Table 3.2.1), we found substantial variance in search coefficients [$4.86 \leq b \leq 4.07 \times 10^3$ ($cm^2\ day^{-1}\ ind^{-q}\ Arena^q$)], handling times [$10^{-3} \leq T_h \leq 9.45 \cdot 10^{-1}$ (day $ind.^{-1}$)], and scaling exponents ($0 \leq q \leq 1.42$). In subsequent

analyses, we related this variance in functional response parameters to predator–prey body-mass ratios spanning roughly three orders of magnitude from 0.65 to 532 (Table 3.2.1).

Table 3.2.1: Mean predator and prey weights, predator–prey body-mass-ratios, and functional response parameters: N = number of replicates, b = search coefficient ($cm^2\ day^{-1}\ ind^{-q}\ Arena^q$), T_h = handling time (day ind.)1), SE = standard error, q = scaling exponent, weight = mean predator weight (mg) and R = predator–prey body-mass ratio

	N	b	SE	T_h	SE	q	SE	Weight	R
Beetles with large prey *Alphitobius diaperinus* [23.26 mg]									
Anchomenus dorsalis	3	0	0	0	0	0	0	14.50	0.65
Calathus melanocephalus	3	0	0	0	0	0	0	17.54	0.79
Calathus fuscipes	36	$9.33*10^2$	$1.39*10^{-3}$	0.52	0.07	0	0.0	71.52	3.08
Pterostichus oblongopunctatus	30	$3.88*10^3$	$1.27*10^{-2}$	0.62	0.06	0	0.0	69.65	2.99
Harpalus rufipes	48	$1.76*10^3$	$3.73*10^{-3}$	0.41	0.06	0	0.0	129.10	5.55
Pterostichus melanarius	36	$4.07*10^3$	$7.83*10^{-3}$	0.25	0.02	0	0.0	158.02	6.79
Abax parallelepipedus	24	$1.49*10^3$	$1.01*10^{-3}$	0.10	0.01	0	0.0	302.00	12.98
Carabus nemoralis	42	$2.98*10^2$	$8.62*10^{-4}$	0.06	0.02	0.11	0.7	513.14	22.06
Beetles with small prey Drosophila hydei [1.42 mg]									
Anchomenus dorsalis	57	$3.63*10^1$	$1.48*10^{-4}$	0.21	0.03	0.86	1.1	14.49	10.21
Calathus melanocephalus	57	$8.52*10^1$	$2.99*10^{-4}$	0.20	0.02	0.68	1	17.54	12.35
Calathus fuscipes	46	4.86	$2.00*10^{-5}$	0.10	0.01	1.42	0.8	81.82	57.62
Pterostichus oblongopunctatus	45	$2.53*10^1$	$7.60*10^{-5}$	0.12	0.01	1.08	0.7	65.05	45.81
Harpalus rufipes	54	$1.49*10^2$	$3.03*10^{-4}$	0.06	0.01	0.54	0.5	41.85	29.47
Pterostichus melanarius	54	$4.78*10^1$	$1.44*10^{-4}$	0.04	0.01	0.53	0.5	148.03	104.3
Abax parallelepipedus	90	$5.07*10^1$	$3.27*10^{-7}$	0.02	$2*10^{-3}$	1.41	0.7	287.58	202.5
Carabus nemoralis	76	$3.32*10^1$	$3.01*10^{-7}$	$5*10^{-3}$	0.01	0.68	0.7	463.84	326.7
Spiders with large prey Drosophila hydei [1.42 mg]									
Pardosa lugubris	54	$1.50*10^3$	$8.25*10^{-3}$	0.14	0.02	0.26	1.9	29.37	20.68
Trochosa terricola, 3 mg	42	$1.22*10^3$	$1.64*10^{-3}$	0.94	0.09	0	0	3.45	2.42
Trochosa terricola, 10 mg	36	$1.90*10^3$	$4.72*10^{-3}$	0.47	0.06	0	0	11.41	8.03
Trochosa terricola, adult	70	$2.07*10^2$	$4.71*10^{-4}$	0.03	$4*10^{-3}$	0.40	0.4	84.81	59.72
Spiders with small Heteromorus nitidus [0.15 mg]									
Pardosa lugubris	60	$1.27*10^1$	$3.90*10^{-5}$	0.05	0.01	1.10	0.6	25.77	171.8
Trochosa terricola, 3 mg	48	$3.43*10^2$	$6.76*10^{-4}$	0.10	0.01	0.5	0.7	3.08	20.51
Trochosa terricola, 10 mg	60	$1.27*10^2$	$3.25*10^{-4}$	0.02	0.01	0.40	0.5	10.61	70.75
Trochosa terricola, adult	88	$7.66*10^1$	$1.73*10^{-4}$	0.01	$1*10^{-3}$	0.10	0.3	79.79	532.4

The handling time exhibited a power-law decrease with increasing predator mass with an exponent of -0.94 ± 0.09 (mean ± SE, Fig. 3.2.1a) and a power-law increase with prey mass with an exponent of 0.83 ± 0.07. We caution, however, that these analyses are based on only three prey size classes and the latter exponent illustrates the relationship only qualitatively. Together, predator and prey mass explained 89% of the variation in handling time. The search

coefficient followed a hump-shaped relationship with predator-prey body-mass ratios (Fig. 3.2.1b, r^2 = 0.74). The hump-shaped nature of this relationship depends on two data points with $\log_{10}$ mass ratios smaller than 0.5 (Fig 3.2.2b), but other predator species in this body-mass range have not been available. The maximum search coefficient, b_{max} = 2161.5, was reached at intermediate body-mass ratios of R_0 = 3.15 (i.e. predators are roughly three times larger than their prey). As handling time is proportional to the inverse of the predators' maximum consumption rates, the maximum nonlinear interaction strengths increase with the body-mass ratios (Fig 3.2.2). These maximum nonlinear interaction strengths are realized at the highest prey densities. At lower prey densities, the nonlinear interaction strengths also depend on successful search rates, which causes hump-shaped relationships with body-mass ratios (Fig. 3.2.2). The scaling exponent, q, was significantly higher for beetles and small prey (q = 0.89 ± 0.15, mean ± SE) than for beetles with large prey (q = 0.02 ± 0.11, Fig. 3.2.1c). This indicates that the nonlinear interaction strengths between beetles and their prey were best described by type III functional responses for high predator–prey body-mass ratios when beetles fed on small prey (Fig. 3.2.2c), whereas type II functional responses characterized their interactions under low predator-prey body-mass ratios with large prey (Fig. 3.2.2a). While a similar pattern of type-III functional responses with small prey (high body-mass ratios; q = 0.52 ± 0.16, mean ± SE) and type-II functional responses with large prey (low body-mass ratios; q = 0.17 ± 0.23, mean ± SE) was found for spiders (Fig. 3.2.2d, b), this difference in the scaling exponent was not statistically significant (Fig. 3.2.1c, contrast analysis for spiders: P = 0.17).

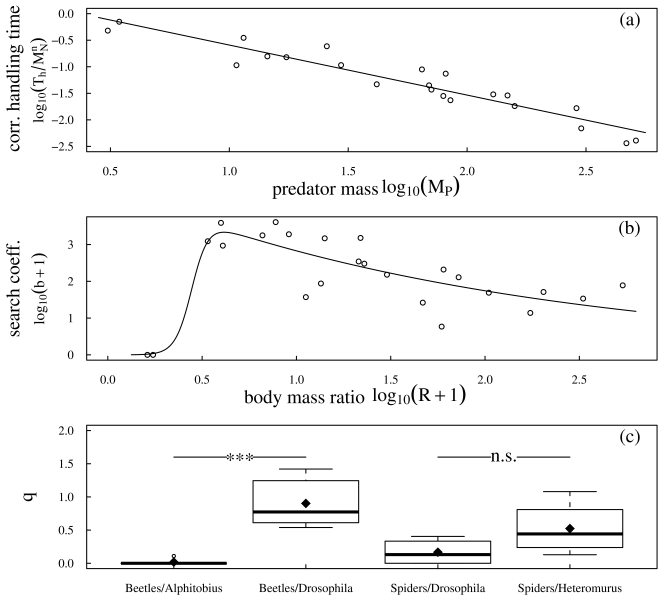

Figure 3.2.1: Allometric scaling of functional response parameters: **(a)** $\log_{10}$ handling time (min ind.$^{-1}$) decreases with $\log_{10}$ predator mass (mg); eqn (4): p = -0.94 ± 0.09 (mean ± SE, P < 0.001), n = 0.83 ± 0.07 (P < 0.001), $T_{h(0)}$ = 0.35 ± 0.14 (P < 0.01), r^2 = 0.887; note that handling time was normalized by the prey body-mass term in Eqn. (3.2.4): $\text{corr}T_h = \log_{10}T_h$) $n\log_{10}M_N$; **(b)** search coefficients (cm^2 day^{-1} ind^{-q} Arena^q) follow a hump-shaped relationship with predator–prey body-mass ratios; eqn (5): A = 3.69 ± 0.52 (P < 0.001), ε = 0.48 ± 0.11 (P < 0.001), F = 0.45 ± 0.154 (P < 0.01) and b = 47.13 ± 88.67 (n.s.), r^2 = 0.74; **(c)** scaling exponents, q, and predator–prey pairs: Beetles / Alphitobius = low body mass ratio, Beetles / Drosophila = high body mass ratio, Spiders / Drosophila = low body mass ratio and Spiders / Heteromurus = high body mass ratio; significant differences among groups according to contrast analyses.

e) Discussion

We studied the influence of predator and prey body masses on 26 functional responses of common terrestrial arthropod predators. We found: (i) power-law scaling in handling times with predator and prey masses, (ii) hump-shaped relationships between search coefficients and predator-prey body-mass ratios, and (iii) increases in the scaling exponent with body-mass ratios (only significant for beetles). Our findings provide evidence of how functional response parameters vary across predator-prey interactions of different body-mass ratios. We focused on two groups of generalist predators with different feeding strategies: beetles are mainly nocturnal, tactile and olfactory, whereas spiders are day active and optically oriented. The similarity in our findings for both predator groups suggests the broad generality of our results.

Interestingly, we found an exponent of -0.94 (SE = ±0.09) in the relationship between handling time and predator body mass, which is significantly different from the exponent of -0.75 initially predicted based on metabolic theory (Peters 1983; Yodzis & Innes 1992; Carbone et al. 1999; Brown et al. 2004). Thus, larger predators had lower handling times and smaller predators had higher handling times than expected based on metabolically driven processes. Assuming that metabolism mainly drives the digestive part of handling, it follows that the speed of morphologically constrained handling processes such as killing and ingesting the prey increases more steeply with predator mass than metabolic processes. For instance, if gut and stomach size are proportional to body size the maximum ingestion will also be proportional to body size. Consequently handling time should be inversely proportional to

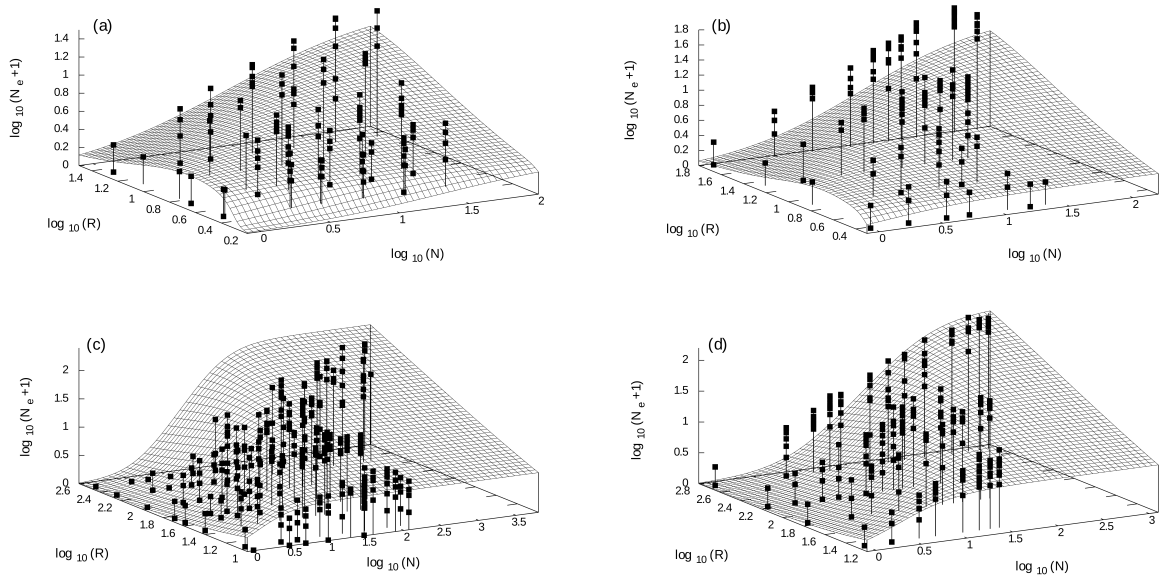

Figure 3.2.2: Experimental per capita consumption rates (N_e) depending on predator–prey body-mass ratios (R) and prey density (N) with allometric functional responses according to the allometric scaling functions of Fig. 3.2.1 for **(a)** Beetles/Alphitobius (low predator–prey body-mass ratios), **(b)** Spiders/Drosophila (low ratios), **(c)** Beetles/Drosophila (high ratios), **(d)** Spiders/Heteromurus (high ratios).

body size, which is consistent with our results. Consistent with most other functional response experiments, the short 24-h time period of our experiments thus emphasizes morphological over digestive constraints on handling times. An improved mechanistic understanding of the scaling exponents thus requires differentiating between ingesting and digesting times in studies with varying experimental duration (Jeschke et al. 2002). While metabolic arguments suggest power-law scaling of digesting times with predator masses, ingesting times could be inversely proportional to body mass.

Instead of the expected linear increase in handling time with prey mass (exponent of unity), we found a scaling exponent of 0.83 ± 0.07 (mean ± SE). One plausible but speculative explanation for this difference could be that the energy content of the prey does not increase proportional to the prey mass. In this case, larger prey would contain more indigestible body parts (e.g. exoskeleton) that impose limitations on ingesting or digesting the prey body. However, a detailed analysis of the morphological and energetic structure of the prey biomass was beyond the scope of the present study. Moreover, we caution that our results were based on only two prey types for each of the predator groups, which may confound the prey-mass scaling relationships presented here. While our study demonstrates that handling time-scales with prey mass, subsequent studies should include a broader variation in prey body masses to more specifically address the exact exponent of this scaling relationship.

Consistent with prior studies investigating search coefficients at constant prey densities (Wahlström et al. 2000; Brose et al. 2008), our results corroborate the hump-shaped relationship between search coefficients and predator-prey body-mass ratios (Figs 3.2.1b and 3.2.2). While the present study was lacking data of direct behavioural observations, we follow prior studies in suggesting that the following behavioural constraints could be responsible for this hump-shaped relationship. Small predators (with low predator-prey body-mass ratios) have a small search area, and they have difficulties in subduing prey larger than themselves leading to inefficient attacks. Large predators (with high predator-prey body-mass ratios) have difficulties in catching small prey individuals, since the much smaller prey have faster reaction times and high escape efficiencies (Brose et al. 2008). At intermediate predator-prey body-mass ratios, however, the highest search coefficients were found, because predators are less restricted in subduing or catching the prey individuals. While the hump-shaped scaling of search coefficients with predator-prey body-mass ratios is supported by our data, these behavioural constraints remain hypotheses to be tested.

In our study, the two different predator groups were most efficient at a predator-prey body-mass ratio of $R_0 = 3.15$ (i.e. when predators were roughly three times larger than their prey). In a prior study, however, the group-specific capture mechanism of predators (e.g. sit-and-move vs. chasing predators) was shown to have a large effect on the optimum predator-prey body mass ratio (Troost, Kooi, & Dieckmann 2008) suggesting that the optimum body-mass ratio

documented here for epigeic spiders and beetles should not necessarily apply to other predator groups. Interestingly, in other ecosystems, a negative relationship between prey density and search rates could occur if the prey employs group defence mechanisms such as swarming (e.g. mammals or fish) (Jeschke & Tollrian 2005). With respect to defence mechanisms of prey, the prey type may thus also influence these scaling relationships.

Moreover, prior studies reported maximum search coefficients of differently sized perch at R_0 = 49.8 for planktonic prey of 0.5 mm and at R_0 = 78.9 for prey of 1 mm size (Wahlström et al. 2000), and R_0 = 103.1 for wolf spiders and R_0 = 83.1 for ground beetles in terrestrial ecosystems (Brose et al. 2008). These studies were based on the simplifying assumption of constant prey densities, whereas the present study overcame this assumption by varying prey densities to estimate search rates of functional responses. While our results support the predicted hump-shaped search rates under varying prey densities, they also demonstrate that optima in the search coefficients were realized at body-mass ratios of R_0 = 3.15, which is approximately one order of magnitude lower than the optimum body-mass ratios of a prior study with the same species (R_0 of 83.1 or 103.1; Brose et al. 2008). This difference suggests that studies at constant prey densities might yield inaccurate estimates of optimum body-mass ratios. Interestingly, the optimum body-mass ratio of the present study is highly consistent with the geometric average body-mass ratio of 3.98 between invertebrate predators and their prey found in terrestrial food webs (Brose et al. 2006a). This implies that many interactions in terrestrial communities might be realized with maximum instantaneous search rates.

Consistent with prior studies, our results suggest that predators efficiently exploit prey within a specific size range. While our present results suggest that terrestrial predators are less specialized than previously anticipated (Brose et al. 2008), striking differences in optimum body-mass ratios, R_0, between these studies are evident. Disentangling whether these differences depend on the organisms investigated (e.g. beetles and spiders vs. fishes) or on ecosystem characteristics (terrestrial vs. pelagic) would require additional studies of varying predator groups in different ecosystem types. Eventually, these studies will allow addressing evolutionary and ecologically relevant questions of different optimum body-mass ratios and degrees of specialization across organism groups and ecosystem types.

In this study, we present evidence from systematic laboratory experiments that the scaling exponent, q, may increase with the predator-prey body-mass ratio, though this difference was only significant for ground beetles. This corroborates prior findings that type III functional responses could occur more frequently than previously anticipated (Sarnelle & Wilson 2008). Interestingly, a similar increase in the scaling exponent with prey size was reported based on gut content analysis of marine minke whales (Smout & Lindstrom 2007). Together, these results could indicate a potentially broad universality of increases in scaling exponents with predator-prey body-mass ratios across different ecosystems.

It has been stressed that functional response experiments should apply a realistic habitat structure in the experimental arenas to create more natural experimental settings, since prey density often also relates to habitat structure (Real 1977; Crawley 1992). Moreover, it was hypothesized that adding such habitat structure could lead to a change of the functional response type as a consequence of potential hiding refuges for the prey (Real 1977; Hassell, Lawton, & Beddington 1977; Crawley 1992). Accounting for this fact, our experimental design included a constant density of moss as a natural habitat structure. Certainly, it would be important to replicate the functional responses of the present study across different moss densities to address how the body-mass effects documented here interact with effects of habitat complexity. Thus, the scaling exponents and attack coefficients of the present study should be interpreted only qualitatively, because different levels of habitat complexity should affect the absolute values of these parameters.

As a general, qualitative pattern, we found that this moss provided refuges for small prey from predation by large predators (high body-mass ratios) resulting in sigmoid, type III functional responses with scaling exponents higher than zero. In contrast, predators of similar body mass as their prey (i.e. low body-mass ratios) were able to follow the prey into the hiding places within the habitat structure resulting in functional responses of type II with scaling exponents of zero. These observations during the experiments provide an explanation for the observed shift from functional responses of type II at low predator-prey body-mass ratios to functional responses of type III at high predator-prey body-mass ratios.

Interestingly, this suggests that population dynamics are stabilized by increasing body-mass ratios as a result of increasing scaling exponents (Oaten & Murdoch 1975a, b; Williams & Martinez 2004a; Brose et al. 2006b; Rall et al. 2008). While previous studies documented that high body-mass ratios stabilize population and food-web dynamics via reductions in the per unit biomass rates of metabolism and consumption (Emmerson & Raffaelli 2004; Brose et al. 2006a; Brose 2008), the increases in the scaling exponent documented here suggest an additional mechanism of how high body-mass ratios stabilize natural ecosystems.

We have presented the scaling of functional response parameters with predator and prey body masses with quantitative parameter estimates. This might be interpreted as an opportunity to estimate quantitatively functional responses based on body masses. However, we caution that this would be a misuse of our model: even in the case of the functional responses of the present study (Table 3.2.1) backward estimation of the per capita consumption rates based on the allometric functional response model yields substantial over- or under-estimations (Fig. 3.2.2). As other scaling models such as species-area relationships or metabolic scaling theory, the results presented here should be interpreted as a documentation of patterns across a body-mass scale. For instance, nobody would seriously estimate the species richness of Borneo based on a global species–area relationship, whereas this scaling

model certainly has a tremendous value as conceptual cornerstone of biogeography. In the same vein, we suggest using the allometric functional response model presented here as an indication of scaling behaviour in foraging ecology. Integrating these scaling relationships into population models will allow predicting general trends in energy fluxes (Brose 2008), food-web structures (Petchey et al. 2008), and the distribution of interaction strengths across food-web links (Bersier et al. 2002). Eventually, combining allometric functional response models with those of food-web structure (Williams & Martinez 2000; Cattin et al. 2004; Petchey et al. 2008) may allow a more detailed understanding how the distribution of body masses across species in natural ecosystems determines population and food-web stability (Brose et al. 2006b; Otto et al. 2007; Rall et al. 2008).

3.3. Allometric degree distributions facilitate food web stability

In natural ecosystems, species are linked by feeding interactions that determine energy fluxes and create complex food webs. The stability of these food webs (de Ruiter et al. 2005; Montoya et al. 2006) enables many species to coexist and to form diverse ecosystems. Recent theory finds predator–prey body-mass ratios to be critically important for food-web stability (Emmerson & Raffaelli 2004; Loeuille & Loreau 2005; Brose et al. 2006b). However, the mechanisms responsible for this stability are unclear. Here we use a bioenergetic consumer–resource model (Yodzis & Innes 1992) to explore how and why only particular predator–prey body-mass ratios promote stability in tri-trophic (three-species) food chains. We find that this 'persistence domain' of ratios is constrained by bottom-up energy availability when predators are much smaller than their prey and by enrichment-driven dynamics when predators are much larger. We also find that 97% of the tri-trophic food chains across five natural food webs (Brose et al. 2005a) exhibit body-mass ratios within the predicted persistence domain. Further analyses of randomly rewired food webs show that body mass and allometric degree distributions in natural food webs mediate this consistency. The allometric degree distributions hold that the diversity of species' predators and prey decreases and increases, respectively, with increasing species' body masses. Our results demonstrate how simple relationships between species' body masses and feeding interactions may promote the stability of complex food webs.

Natural food webs are characterized by energy and biomass flows across various trophic levels. Despite the structural complexity of these large networks (Williams & Martinez 2000), simple food-chain motifs usefully represent the energy transfer (Milo et al. 2002; Bascompte & Melian 2005) and mechanisms responsible for non-equilibrium population dynamics in food webs (Hastings & Powell 1991; Muratori & Rinaldi 1992; Jonsson & Ebenman 1998; McCann et al. 1998). Analyses of food-chain motifs illustrate how population stability under chaotic dynamics may be driven by high resource productivity (Hastings & Powell 1991), variation in the species' timescales (Muratori & Rinaldi 1992) or certain body-mass ratios between consumers and resources (Jonsson & Ebenman 1998). Population persistence depends on parameters of energy gain (production and consumption) and loss (metabolism and mortality) (Gard 1980), whose rates per unit biomass follow allometric negative-quarter power-law relationships with the average body masses of the populations (Brown et al. 2004; Savage, Gillooly, Brown, et al. 2004). We use a bioenergetic model based on these principles (Yodzis & Innes 1992) to explore how the dynamics of top (t), intermediate (i) and basal (b) species of tri-trophic food chains changes with varying consumer–resource body-mass ratios

(*R*). Our analyses predict the probability of stable coexistence of three invertebrate species in tri-trophic food chains depending on *R*, which is subsequently evaluated for food chains of five natural food webs (Brose et al. 2005a).

We initially explored a tri-trophic system by simultaneously increasing *R* between top and intermediate species (R_{ti}) and between intermediate and basal species (R_{ib}) from 10^{-8} to 10^{8} (that is, the consumer is between 10^{8}-fold smaller and 10^{8}-fold larger than its prey). The simultaneous increase in both *R* values is a simplification to gain knowledge of the population dynamics. The minima and maxima attained for the biomass densities of the three species across this range of *R* (Fig. 3.3.1a–c) depict four distinct stages of coexistence. At the lowest *R* ($R = 10^{-6.7}$), the system exhibits a stable equilibrium where only the basal species persists. At higher *R* ($10^{-6.7} \leq R < 10^{-1.6}$), two stable attractors appear: either the basal species persists at equilibrium, or basal and intermediate species exhibit globally attractive limit cycles (Muratori & Rinaldi 1992). In this range of *R*, the top species is much smaller than its prey, and its mass-specific metabolic rate exceeds the energy available from consuming the intermediate species, which prevents persistence (Gard 1980). Increasing *R* above these low ratios decreases the metabolic rates per unit biomass of top and intermediate species and increases the intermediate species' biomass density until the top species' consumption exceeds its metabolic demand enough for the top species to persist ($R = -10^{-1.6}$). Further increases in *R* ($10^{-1.6} < R < 10^{3.5}$) increases top-down pressure on the intermediate species and decreases top-down pressure on the basal species (Fig. 3.3.1d). Increasing *R* within this range also increases the consumption rate per unit biomass of the intermediate species over that of the top species (Fig. 3.3.1e). This counter-intuitive result is explained by the simultaneous decrease in the density of intermediate species and increase in the density of basal species, which enhances the energy availability per unit biomass to the intermediate species. This availability increases with *R*, leading to

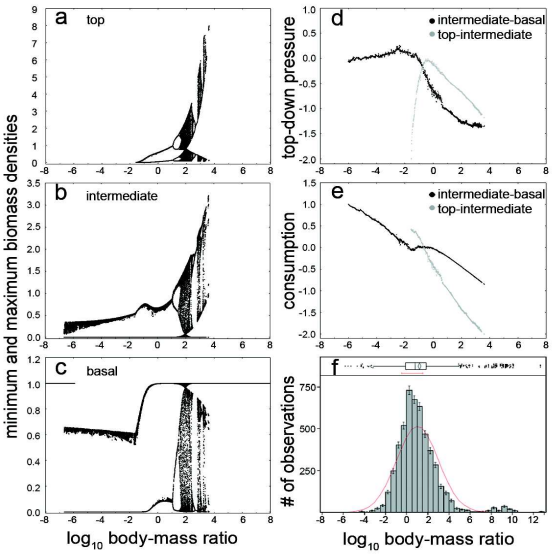

Figure 3.3.1: Population dynamics in tri-trophic food chains. **a–c**, Effects of *R* on the biomass minima and maxima of top **(a)**, intermediate **(b)** and basal **(c)** species. d, Effect of *R* on $\log_{10}$ of top-down pressure per unit biomass of prey, for intermediate–basal (black) and top–intermediate (grey) species. **e**, Effect of *R* on $\log_{10}$ of consumption per unit biomass of predator, for intermediate–basal (black) and top–intermediate (grey) species. **f**, Frequency distribution of empirical *R* in five natural food webs (means ± s.e.m.); the red line shows a normal distribution. An outlier box-plot is shown above the histogram. Simultaneous variation of *R* of top to intermediate and intermediate to basal species: when $R = 0$, all three species have equal size; when $R < 0$ and $R > 0$, predators are smaller and larger, respectively, than their prey.

accelerating oscillations of top and intermediate species (Fig. 3.3.1a–c). Mechanistically similar to the 'paradox of enrichment' (Rosenzweig 1971), the dynamics are driven from equilibrium through a series of bifurcations to more complex dynamics until the minimum density of the intermediate species drops below a critical extinction threshold, eliminating both consumer species ($R = 10^{3.5}$; Fig. 3.3.1). The complex dynamics in this range of R are caused by the different timescales of the three populations (Muratori & Rinaldi 1992). Further increases in R ($R > 10^{3.5}$) cause unstable dynamics that continue to prevent the persistence of the intermediate and top species (Fig. 3.3.1a–c). The persistence of all three species is thus bounded by energy availability to the top species at low R and by enrichment-driven instability of the intermediate species towards higher R.

With this mechanistic background on food-chain dynamics, we decoupled R of upper and lower trophic levels and independently varied both R_{ti} and R_{ib} between 10^{-6} and 10^{13}. This range corresponds to the range of empirical R values of the five natural food webs studied here (Fig. 3.3.1f). In 19.6% of this parameter space, we found persistence of all three species (Fig. 3.3.2, red areas). The energy-availability boundary of this persistence domain depends on R_{ib}, which needs to exceed a threshold ($R_{ib} > 10^{-1.6}$) within a broad range of R_{ti} ($R_{ti} > 10^{-4.3}$) to increase the density of the intermediate species (that is, the energy available) enough for the top species to persist (Fig. 3.3.2, left boundary of red areas). If R_{ib} and R_{ti} exceed a second threshold, both top and intermediate species cease to persist as a result of enrichment-driven dynamics (Fig. 3.3.2, right boundary of red areas). This enrichment boundary is determined more continuously and interactively by both R_{ib} and R_{ti} than the energy-availability boundary (Fig. 3.3.2).

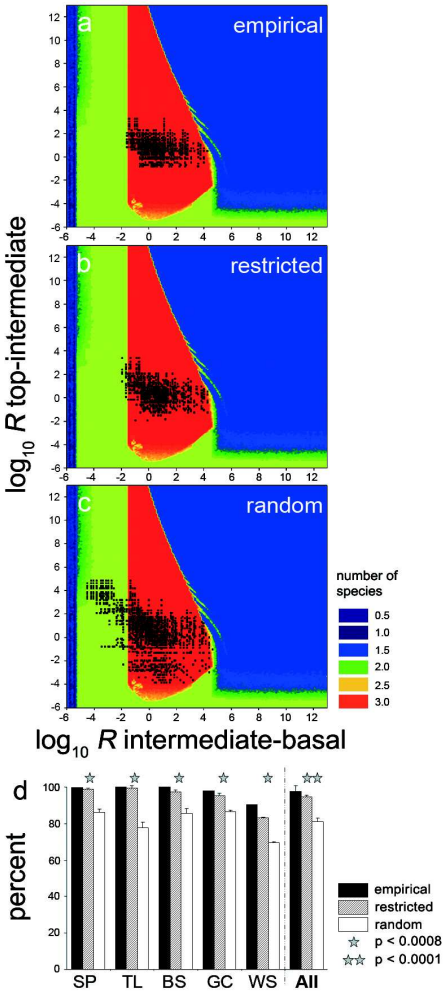

Figure 3.3.2: **Population persistence in tri-trophic food chains depending on R_{ti} and R_{ib}. a–c**, Colours indicate the numbers of persistent species; red areas characterize a tri-trophic 'persistence domain'. Black points represent food chains of Skipwith pond under empirical food web structures **(a)**, restricted rewiring **(b)** and random rewiring **(c)**. **d**, Percentages of food chains within the persistence domain (SP, Skipwith pond; TL, Tuesday lake; BS, Broadstone stream; GC, Grand Cariçaie; WS, Weddell Sea) under empirical structures, restricted and random rewiring; results are shown as means and s.d.. Stars indicate significant differences between the rewired versions of each food web.

The persistence domain in Fig. 3.3.2 implies that a tri-trophic food chain with R randomly chosen from the range $10^{-6} \leq R \leq 10^{13}$ has a 19.6% chance of persisting. However, 97.5% ± 4.1% (mean ± s.d.) of all invertebrate tri-trophic food chains across five natural food webs from different ecosystem types (see Methods) fall within the persistence domain (Fig. 3.3.2a, black points; Fig. 3.3.2d, black bars). This difference in probabilities clearly suggests that species' body-mass distributions in these food webs strongly stabilize food-chain dynamics. To further explore this hypothesis, we randomly rewired the empirical food webs in a way that preserves the body masses of the species and the total number of links while completely disrupting the food-web topology ('random rewiring'; see Methods). An average of 81.0% ±7.0% (mean ± s.d.) of these rewired food chains in each of the five food webs fell within the persistence domain (Fig. 3.3.2c,d, white bars). This probability is 4.1-fold the 19.6% probability of food chains with randomly distributed body masses within empirically observed ranges that are systematically and independently linked. However, 81% is significantly lower than the 97.5% probability that empirical food chains overlap with the persistence domain ($P < 0.01$). This difference suggests that, while the distribution of species' body masses found in natural food webs provides a substantial increase in the dynamical stability of possible food chains, topological properties of actual food chains might further facilitate food-web stability. To explore which topological properties can provide this additional stabilization, we tested whether correlations between the body mass and degree of species (that is, the number of predator and prey links of a population) drive this effect. To do this, we randomly rewired the food webs with a second randomization algorithm that preserves the body mass and degree of each species ('restricted rewiring'; see Methods). An average of 94.7% ±6.2% (mean ± s.d.) of the food chains rewired in this restricted way lie within the persistence domain (Fig. 3.3.2b,d, grey bars). This probability is 4.8-fold the probability of food chains with randomly distributed body masses (19.6%) and differs significantly from randomly rewired networks (81.0%, $P < 0.05$), but it is not significantly lower than that in empirical food chains (97.5%, $P > 0.17$).

Overall, our results suggest that the distributions of and correlations between the body mass and degree of species within food webs are important mechanisms responsible for food-chain stability. Other topological properties of food webs seem to be of more minor importance. Instead, preserving allometric degree distributions realizes probabilities of tri-trophic stability similar to those found in empirical food webs. This conclusion seems qualitatively insensitive to variation in model parameters (see Supplementary Information). In the five natural food webs studied, the critically important mass–degree relationships are characterized by significant decreases in the number of predator links and significant increases in the number of prey links with increasing body masses of species (Table 3.3.1). These simple relationships were removed in the random procedure and retained in the restricted-rewiring procedure (Table 3.3.1). Our results seem to reveal a mechanistic basis of

body-mass effects on population persistence in simple tri-trophic food chains. Scaling up our analyses to complex food webs suggests that population persistence there could be determined by similar constraints (see Supplementary Information). Although domains of stability using other functional responses also need to be explored, our results for the most widely used nonlinear functional response are of broad importance to ecology. Future extensions of our approach need to also address more variation between network models, species numbers and metabolic types of species to illuminate the generality of the results described here.

Table 3.3.1: Allometric degree distributions: dependence of species' link structures (y) on body mass (x)

Food web	Topology	y	Regression equation	R^2	n	P
Skipwith Pond	Empirical	No. of predators	$y = -1.00 \log x + 5.91$	0.21	33	0.01
		No. of prey	$y = 2.47 \log x + 21.01$	0.26	33	0.003
	Random	No. of predators	$y = -0.26 \log x + 9.13$	0.05	33	0.20
		No. of prey	$y = -0.08 \log x + 9.94$	0.004	33	0.71
Tuesday lake, 1984	Empirical	No. of predators	$y = -0.19 \log x + 1.57$	0.47	25	0.0002
		No. of prey	$y = 0.71 \log x + 12.61$	0.35	25	0.002
	Random	No. of predators	$y = -0.03 \log x + 3.50$	0.01	25	0.58
		No. of prey	$y = 0.03 \log x + 4.30$	0.007	25	0.69
Broadstone stream	Empirical	No. of predators	$y = -0.80 \log x - 1.91$	0.40	29	0.0003
		No. of prey	$y = 1.44 \log x + 17.76$	0.15	29	0.04
	Random	No. of predators	$y = 0.31 \log x + 7.85$	0.10	29	0.10
		No. of prey	$y = -0.24 \log x + 3.02$	0.10	29	0.10
Grand Caricaie, ClControl 2	Empirical	No. of predators	$y = -0.54 \log x + 4.39$	0.13	102	0.0002
		No. of prey	$y = 0.61 \log x + 11.59$	0.05	102	0.03
	Random	No. of predators	$y = -0.06 \log x + 7.36$	0.01	102	0.45
		No. of prey	$y = -0.05 \log x + 7.44$	0.004	102	0.51
Weddell Sea shelf	Empirical	No. of predators	$y = -0.44 \log x + 16.93$	0.02	275	0.03
		No. of prey	$y = 1.96 \log x + 20.64$	0.10	275	< 0.0001
	Random	No. of predators	$y = 0.04 \log x + 17.68$	0.002	275	0.50
		No. of prey	$y = 0.01 \log x + 17.64$	0.0003	275	0.59

Linear least-square regressions of the number of predators and prey per species (y) on the $\log_{10}$ body masses (x) of the species of five food webs under empirical food-web structures and randomly rewired networks. Empirical networks and restricted rewired networks (not shown) show similar degree distributions, because the restricted rewiring algorithm preserves the number of predators prey per species; n is the number of invertebrate species in the food web.

Community stability is known to be critically dependent on the body-mass distribution within food webs (Emmerson & Raffaelli 2004; Loeuille & Loreau 2005; Brose et al. 2006b). Here we explore potential mechanisms behind these stability effects by simulating tritrophic food chains whose persistence is possible under a limited combination of species' body masses that describe a persistence domain. These mechanisms include energy limitation of the top species when predators are much smaller than their prey, and unstable enrichment-driven

dynamics of intermediate species when they are much larger. Tri-trophic food chains are frequently parts of more complex motifs within food webs (Milo et al. 2002; Bascompte & Melian 2005) that may exhibit more stable dynamics (McCann et al. 1998; Fussmann & Heber 2002) or gain additional stability if large top predators couple either spatially separated food chains or other fast and slow energy channels (Koelle & Vandermeer 2005; McCann, Rasmussen, & Umbanhowar 2005; Rooney et al. 2006). Although ignoring such additional model complexity, the persistence domain predicted by our food-chain model is matched surprisingly well by 97.5% empirical food chains across five natural food webs. Further work on more complex food-web motifs is needed to obtain a better understanding of how body-mass dependent population persistence scales up with system size from food chains to food webs.

Body masses impose physical constraints on who can hunt, handle and ingest whom in a community (Woodward et al. 2005; Brose et al. 2006a), which determines the diet breadth and foraging behaviour of individual species and topological food-web parameters (Jonsson, Cohen, & Carpenter 2005; Loeuille & Loreau 2005; Beckerman et al. 2006). To these relationships between body size and food webs, our study adds allometric degree distributions in which larger species feed on more prey and are consumed by fewer predators than small species. Our study provides a possible explanation for how these distributions may affect characteristics such as population persistence and food-web stability in natural communities. This connection between community-level degree distributions (Montoya & Solé 2003; Stouffer et al. 2005) and population biology suggests a fundamental bridge between food-web structure (Williams & Martinez 2000; Cattin et al. 2004; Stouffer et al. 2005) and food-web dynamics (Loeuille & Loreau 2005; Brose et al. 2006b). Our results illuminate an allometric mechanism that may help to maintain the critically important biodiversity of natural ecosystems.

a) Methods Summary

Simulations.

A bioenergetic population dynamics model (Yodzis & Innes 1992) defines the biomass evolution, dB/dt, of basal (b), intermediate (i) and top (t) species:

$$\frac{dB_b}{dt} = r_b G_b B_b - \frac{x_i y_i F_{ib} B_i}{e} \qquad (3.3.1a)$$

$$\frac{dB_i}{dt} = -x_i B_i + x_i y_i F_{ib} B_i - \frac{x_t y_t F_{ti} B_t}{e} \qquad (3.3.1b)$$

$$\frac{dB_t}{dt} = -x_t B_t + x_t y_t F_{ti} B_t \qquad (3.3.1c)$$

where e is the assimilation efficiency, G_b is the logistic net growth (with carrying capacity K) and F is a type II functional response. Biological rates r, x and y (growth, metabolism and maximum consumption) scale with body mass, M: $r, x, y \propto M^{-0.25}$. r, x, y were normalized to the growth rate of basal species (thus, $r_b = 1$), and y was normalized to x. The maximum consumption rate was constant ($y = 8$); x increased with the body-mass ratio to basal species:

$$x_{i,t} = a\left(\frac{M_{i,t}}{M_b}\right)^{-0.25}$$

where a is a constant ($a = 0.2227$ when top, intermediate and basal species are invertebrates (Brown et al. 2004)). $R_{ti} = M_t / M_i$ and $R_{ib} = M_i / M_b$ are varied between 10^{-8} and 10^{13},which influences their rates of metabolism (x) and consumption (xyF) per unit biomass. Initial biomass densities were random, simulations were run over 100,000 time steps. Maximum and minimum biomass densities of persistent populations ($B > 10^{-30}$) were recorded, and combinations of persistent R_{ti} and R_{ib} were defined as a 'persistence domain'. The averages of the top-down pressure per unit biomass on basal and intermediate species are $P_{b,i} = x_{i,t}\, y_{i,t}\, F_{ib,ti}\, B_{i,t} / B_{b,i}$, and the energy fluxes per unit biomass to intermediate and top species are $E_{i,t} = x_{i,t}\, y_{i,t}\, F_{ib,ti}$.

Rewiring

We compared R_{ti} and R_{ib} of the persistence domain with those of all tri-trophic food chains from five natural food webs (see Table 3.3.1) (Brose et al. 2005a). We created two additional versions of each empirical food web under random and restricted rewiring. For each treatment we calculated the fraction of food chains that were located within the persistence domain of our simulations under three conditions: empirical food web structures, restricted rewiring and random rewiring. Differences in results were evaluated by independent Mann–Whitney U-tests. Relationships between the degree and body mass of species were analysed by ordinary linear least-square regressions.

b) Full Methods

Model

Population dynamics of three invertebrate species in a food chain follow a bioenergetic model (Yodzis & Innes 1992) of the biomass evolution (see Eqn. (3.3.1)). $G_b = 1 - B_b / K$ and $F_{ib} = B_b / (B_0 + B_b)$; $F_{ti} = B_i / (B_0 + B_i)$ with a half saturation density B_0. Here, the fraction of

the biomass removed from the resource population that is actually eaten is set to unity, which is often characterized as the mechanistically simplest model of predator–prey interactions (Jeschke et al. 2002). The biological rates of production (W), metabolism (X) and maximum consumption (Y) follow negative quarter power-law relationships with the species' body masses (Brown et al. 2004):

$$W_b = a_r M_b^{-0.25} \tag{3.3.2a}$$

$$X_{i,t} = a_x M_{i,t}^{-0.25} \tag{3.3.2b}$$

$$Y_{i,t} = a_y M_{i,t}^{-0.25} \tag{3.3.2c}$$

where a_r, a_x and a_y are allometric constants (Yodzis & Innes 1992). The timescale of the system is defined by setting the mass-specific growth rate to unity (Eqn. 3.3.3a). Then the mass-specific metabolic rates of all species, x, are normalized by the timescale (Eqn. 3.3.3b), and the maximum consumption rates, y, are normalized by the metabolic rates:

$$r_i = 1 \tag{3.3.3a}$$

$$x_{i,t} = \frac{X_{i,t}}{W_b} = \frac{a_x}{a_r}\left(\frac{M_{i,t}}{M_b}\right)^{-0.25} \tag{3.3.3b}$$

$$y_{i,t} = \frac{Y_{i,t}}{X_{i,t}} = \frac{a_y}{a_x} \tag{3.3.3c}$$

Substituting equations (3.3.3a)–(3.3.3c) into equations (3.3.1a) and (3.3.1b) yields a population dynamic model with allometrically scaled and normalized parameters. Here the body mass of the basal species, M_b, is set to unity, and the body masses of all other species, M_i and M_t, are expressed relative to the body mass of the basal species. This makes the results presented here independent of the body mass of the basal species.

Simulations

In simulations of tri-trophic food chains, the R values between the top and intermediate species (R_{ti}) and between the intermediate and basal species (R_{ib}) define the body masses M_i and M_t. We used constant values for the other model parameters: maximum ingestion rate $y_{i,t}$ = 8 for invertebrate predators; assimilation efficiency e = 0.85 for carnivores; carrying capacity K = 1; half saturation density of the functional response B_0 = 0.5; allometric constant $a = a_x / a_r$ = 0.2227 (top, intermediate and bottom species were simulated as invertebrates). We sought a mechanistic explanation for the influence of R on food-web stability by simulating food chains as the simplest multitrophic motif with energy transfer across several trophic levels. This characterizes complex natural food webs better than bitrophic consumer–resource

relationships. Analyses of more complex motifs such as omnivory modules require knowledge about the relative interaction strengths of generalist predators with their multiple prey, which was not available for the natural food webs studied. We varied R between the top and intermediate species ($R_{ti} = M_t / M_i$) and between the intermediate and basal species ($R_{ib} = M_i / M_b$) between 10^{-8} and 10^{13}, which decreased their rates of metabolism (x) and consumption (xyF) per unit biomass. Simulations started with uniformly random biomass densities ($0.05 < B_{t,i,b}\ (T{=}0) < 1$) and ran more than 100,000 time steps (T) or until the largest species attained two biomass minima. We recorded the maximum and minimum biomass densities in the second half of the time series of the persistent populations ($B > 10^{-30}$) and defined a 'persistence domain' of combinations of R_{ti} and R_{ib} that enabled persistence of the three populations. For every time series we calculated the averages of the top-down pressure per unit biomass on the basal species, $P_b = x_i\, y_i\, F_{ib}\, B_i / B_b$, and the energy flux per unit biomass to the intermediate species, $E_i = x_i\, y_i\, F_{ib}$. Similar calculations yield the averages of the top-down pressure per unit biomass on the intermediate species and the energy flux per unit biomass to the top species.

Evaluation and rewiring

Subsequently, we compared the R_{ti} and R_{ib} values of the persistence domain with those of all tri-trophic food chains across five natural food webs: one from a stream (**Broadstone stream**), one from a pond (**Skipwith pond**), one from a lake (**Tuesday lake, 1984**), one terrestrial (**Grand-Cariçaie, ClControl2**) and one marine (**Weddell Sea shelf**) from a global data base (Brose et al. 2005a). To allow comparisons with our simulations, we studied only food chains of three invertebrate species that composed the vast majority of food chains in the empirical food webs, whereas few food chains include vertebrates or plant species. To test our hypotheses we created two additional versions of each of these empirical food webs under random and restricted rewiring. The 'random rewiring' algorithm conserved only the species' body masses and the total number of links, n, of the empirical food webs and randomly relinked n species pairs without any restrictions. The 'restricted rewiring' algorithm (see (Milo et al. 2002) and references therein) randomly selects two predator–prey pairs and reconnects the predator of the first pair with the prey of the second pair and vice versa. This rewiring required that none of the new links already existed and ensured the conservation of the total number of predators and prey of each species along with their body masses and the total number of links in the network. We relinked n pairs of links in each food web 20 times to create a random rewired version of the network. Each of the two algorithms was applied to each of the five food webs studied with eight replicates. For each replicate we calculated the fraction of invertebrate food chains with body-mass ratios that were located within the persistence domain of our simulations under three conditions: empirical food web structures,

restricted rewiring and random rewiring. Statistics. Differences in these fractions between the three versions of the food webs were statistically evaluated by eight independent Mann–Whitney U-tests. In each test the five empirical probabilities were tested against five probabilities for each rewiring algorithm (randomly drawn from the eight replicates for each food web). Subsequently, each test was characterized by the highest of the eight *P* values. The relationships between the numbers of predator links and prey links and the body masses of the species were analysed by ordinary linear least-square regressions. Regressions were performed for each empirical replicate and one randomly rewired replicate of each of the five food webs.

c) Supplementary Information

In this study, we analyze the stability of tri-trophic food chains depending on varying body-mass ratios between the top and intermediate species, R_{ti}, and between the intermediate and basal species, R_{ib}. For our dynamical simulations, we use a bioenergetic model with allometrically scaling parameters (Yodzis & Innes 1992) to show how the dynamics and energetic relationships between the three species of the food chains change with varying consumer-resource body-mass ratios. Subsequently, we present (1) additional numerical simulations to provide a parameter sensitivity analysis, (2) methods of complex food-web

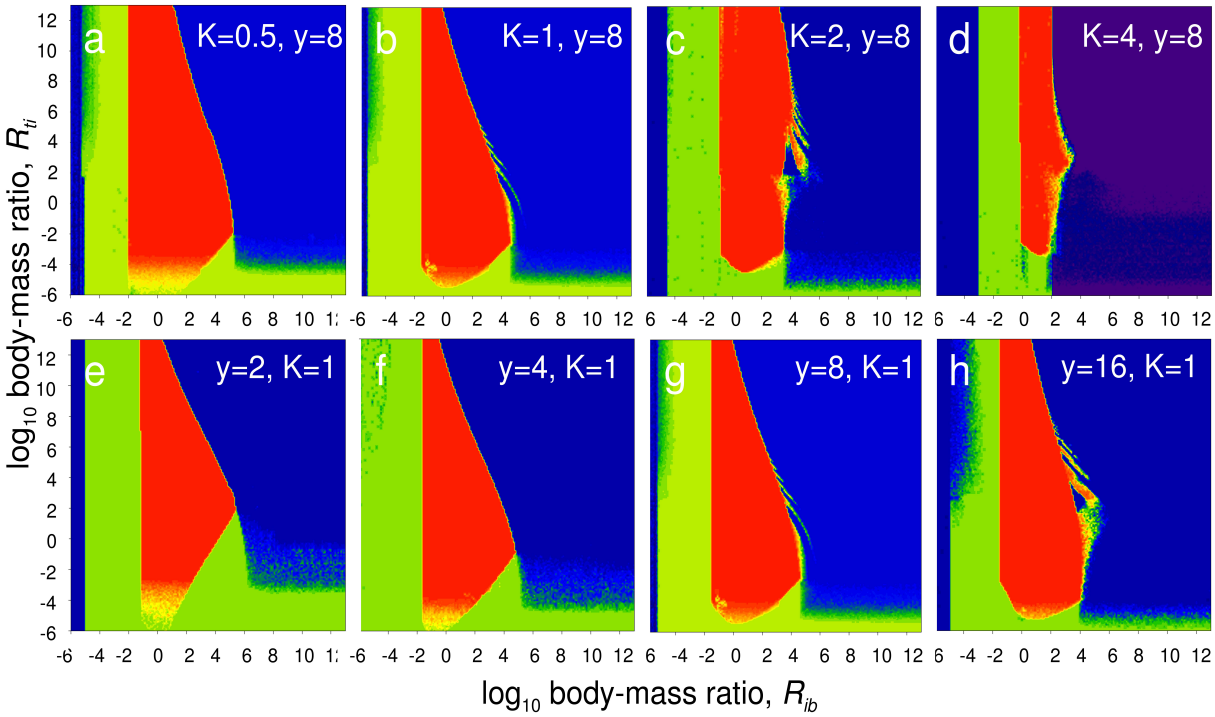

Supplement Figure 3.3.3: The size and shape of the 'persistence domain' (red areas) depends on **A**-**D**) the carrying capacity of the system, *K* (here with constant *y* = 8), but varies only marginally with **E**-**H**) the maximum ingestion rate of the consumers, *y* (here with constant *K* = 1).

simulations and (3) analyses of complex food-webs.

Supplementary Figures and Legends – Model sensitivity

The metabolic rates of the species follow allometric negative-quarter power-law relationships with the average body masses of the populations (Brown et al. 2004; Savage, Gillooly, Brown, et al. 2004) (see Eqn. 3.3.3b, Full Methods). The parameters of maximum consumption of the consumers, y, the carrying capacity of the basal species, K, half saturation density of the functional response, B_0 and the assimilation efficiency of the consumer species, e, are independent of the body masses, and they were assigned constant values. Following prior work (Yodzis & Innes 1992), we used an empirically supported assimilation efficiency of the consumer species of $e = 0.85$. The maximum per capita interaction strength of a resource species on a consumer species is proportional to y / B_0 see reference (McCann et al. 1998). In our simulations, we used constant values of the carrying capacity ($K = 1$), the maximum consumption of the consumers ($y = 8$) and the half saturation density of the functional response ($B_0 = 0.5$). This parameter set is consistent with simulations in previous work (Brose et al. 2006b). However, the shape and boundaries of the simulated 'persistence domain' (Fig. 3.3.2a, main text) depend on the parameters chosen (Supplement Fig. 3.3.3A-H). Independent of the parameters used, energy limitation of the top species depends on R_{ib} whereas the boundary to unstable enrichment-driven dynamics of the intermediate species is interactively determined by both R_{ib} and R_{ti}. Increasing the carrying capacity, K (Supplement Fig. 3.3.3A-D) is equivalent to increasing the enrichment of the food chains, which leads to a decreasing size of the persistence domain (Supplement Fig. 3.3.3A-D). Increasing the maximum consumption rate, y, causes higher top down pressure by the consumer species, but the effects on the size of the persistence domain are marginal (Supplement Fig. 3.3.3E-H). Note that y equal to one represents a system in which the maximum ingestion rate is equal to the metabolic rate of the consumer. The energy gain by consumption is given by the product of consumption rate and assimilation efficiency ($e = 0.85$). Moreover, at prey densities below infinity, the actual consumption rate is lower than the possible maximum consumption rate. Therefore, systems with a maximum consumption rate of unity are not feasible (Supplement Fig. 3.3.4B). Variation in K is equivalent to variation of the enrichment of the food chain and variation of the maximum ingestion rate alters the maximum per capita interaction strength (y / B_0). As increasing y is qualitatively similar to decreasing B_0, we only varied y in our additional simulations. The percentages of empirical and re-wired food chains within the persistence domain also depend on K and y (Supplement Fig. 3.3.4A, B). However, our general result, that food-chain stability in empirical food-webs and under restricted re-wiring is significantly higher than food-chain stability under random re-wiring of the network structures, holds across the range in K and y in our simulations. For $K > 4$ all food chains are unstable due to too large enrichment (Supplement Fig. 3.3.4A, B).

Supplementary Methods – Complex food-web analyses

Additionally to the food chain analyses, we simulated niche-model food webs (Williams & Martinez 2000) (100 replicates per body-mass ratio) with a species richness of 20 (thereof 5 basal species) and a connectance of 0.15. The trophic levels of a species i is calculated as the prey-averaged trophic level T_i:

$$T_i = 1 + \frac{\sum_{j=1}^{n} T_j}{n} \qquad (3.3.4)$$

where i has n prey species j. In complex food webs with constant predator-prey body-mass ratios, Z, the body masses of basal species are set to unity and the body masses of consumers, M_i, increase with their trophic levels by:

$$M_i = Z^{T_i - 1} \qquad (3.3.5)$$

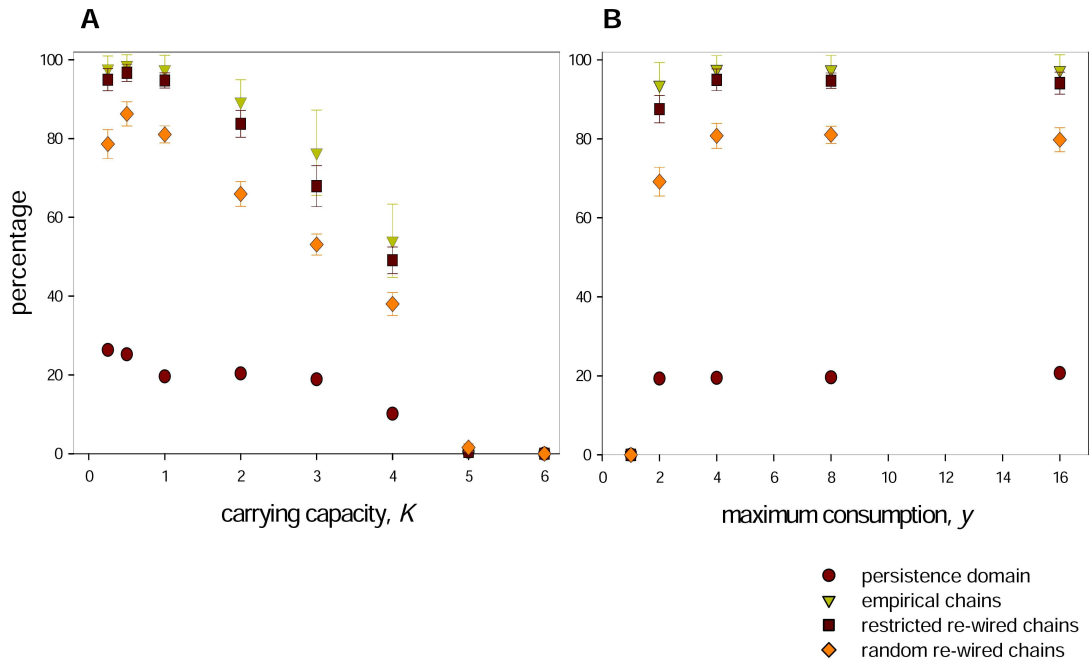

Supplement Figure 3.3.4: The size of the 'persistence domain' (circles, i.e. red areas of Fig. 3.3.2, main text) depends on **A)** the carrying capacity of the system, K and **B)** the maximum ingestion rate of the consumers, y. The number of persistent empirical (triangles) and re-wired food chains (restricted: squares, random: diamonds) falling in the persistence domain (i.e. black points in Fig. 3.3.2, main text) also depends on these parameters. Shown are the mean and 95% confidence interval.

These body masses are used to parameterize the metabolic rates of the bioenergetic model. Thus, knowledge on the trophic levels of the species from the binary feeding matrix predicted by the niche model allows calculating their body-masses relative to the body-mass of the producer species (Eqn. 3.3.4), which parameterizes the parameters of the consumer-resource

model (see main text, Full Methods, Eqn. 3.3.1a-c). We used constant values for the other model parameters: maximum ingestion rate y = 8 for invertebrate predators; assimilation efficiency e = 0.85 for carnivores; carrying capacity K = 1; half saturation density of the Holling type II functional response B_0 = 0.5; allometric constant a = 0.2227 when all species are invertebrates. After simulations over 250,000 time steps, we calculated the fraction of persistent species ($B > 10^{-30}$). We started every individual simulation with a food web stochastically generated by a specific model initialized with uniformly random population densities in terms of biomass density of species i ($0.05 < B_i < 1$) and recorded the number of persistent populations ($B_i > 10^{-30}$) at the end of the time series (t = 250,000). Note that: (i) simulations with shorter time series (e.g. t = 50,000) would yield qualitatively similar results with a slightly higher proportional persistence but would not allow to analyse the dynamics of very large consumer-resource body-mass ratios; and (ii) different extinction thresholds produce qualitatively the same results at different levels of persistence (lower extinction thresholds increase the persistence). We measured the fraction of persistent populations (i.e. species richness persisting at the end of the simulation divided by initial species richness) and the maximum trophic level in the food web (i.e. the maximum of the trophic levels of the populations in the food web).

Supplementary Data, Figures and Legend – Complex food-web analyses

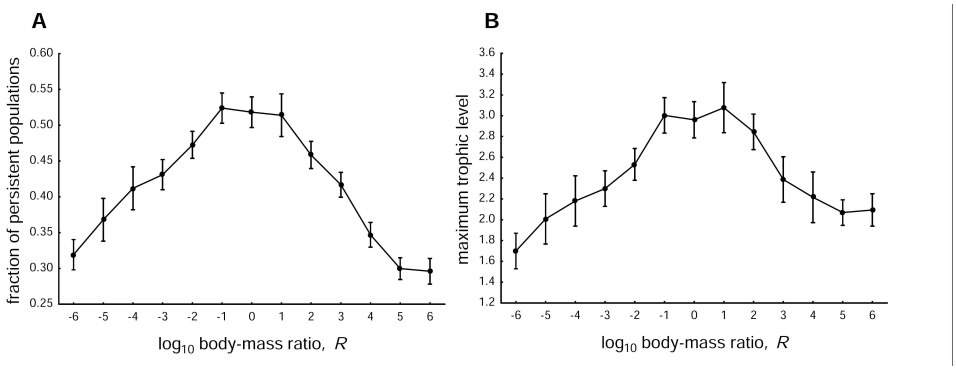

Supplement Figure 3.3.5: Analyses of complex niche-model food webs: **A)** The fraction of initial populations that dynamically persist and **B)** the maximum trophic level amongst the persistent populations depending on the predator-prey body-mass ratios in the food webs. Data points are means and 95% confidence intervals over 100 niche-model food webs of 20 species.

Consistent with the food chain analyses, population persistence in 20-species food-web models first increases and then decreases with predator-prey body-mass ratios, R (Supplement Fig. 3.3.5A). A prior study (Brose et al. 2006b) that averaged results over varying functional responses, network models, species numbers and metabolic types of species found only the increasing population persistence with R of this hump-shaped relationship. This may partially be explained by the fact that networks of higher species richness or those comprised of vertebrate species continue increasing in persistence up to higher body-mass ratios than the

20-species food webs of invertebrates addressed in the present studies. Future studies need to analyse these differences. Despite these quantitative differences, the model presented here addressed the mechanistic basis of body-mass effects on population persistence. Moreover, our results suggest a hump-shaped relationship between the maximum trophic level in the food web and the predator-prey body-mass ratio: maximum trophic levels first increase and then decrease with increasing R in our simulations (Supplement Fig. 3.3.5B). A plateau of maximum trophic levels is reached between body-mass ratios of 10^{-1} and 10^{2}. In this range of R, the average of the maximum trophic level (i.e. the average over 100 niche-model food webs) does not significantly differ from three (i.e. three is within the 95% confidence intervals, Supplemental Fig. 3.3.5B). This suggests that food chains in these simulated food webs may include up to three species, whereas simulated food webs with lower or higher body-mass ratios are restricted to shorter food chains. This suggests that tri-trophic food chains might be restricted to intermediate body-mass ratios in complex food webs, which is consistent with our conclusion in the main text of the manuscript.

3.4. The omnivory conundrum: allometry balances weak and strong interactions in complex food webs

In natural food webs, omnivory motifs – defined as three-species food chains with an additional top-basal link – occur much more frequently than expected by chance (Woodward & Hildrew 2002a; Arim & Marquet 2004; Bascompte & Melian 2005; Stouffer et al. 2007), and their stability is critically important for maintaining community diversity, complexity and functioning (Neutel et al. 2002; Neutel et al. 2007). While omnivory is destabilizing in null models using random combinations of species' interaction strengths (Pimm & Lawton 1978; Holt & Polis 1997; Vandermeer 2006), stability can emerge if the top-basal link is weak compared to the average interaction strength in the food chain (McCann & Hastings 1997; Holt & Polis 1997; McCann et al. 1998; Emmerson & Yearsley 2004). Yet, it has remained elusive as to how natural communities can systematically maintain this highly specific interaction strength distribution, leaving the scientific conundrum of why omnivory motifs are so frequent in natural food webs unresolved1. Here, we analyse a bioenergetic model to show that simple allometric relationships constrain the distribution of weak and strong interactions yielding stable omnivory motifs. These allometry constraints are mediated by (i) a frequently-documented hump-shaped relationship between attack rates and predator-prey body-mass ratios (Wahlström et al. 2000; Aljetlawi et al. 2004; Vonesh & Bolker 2005; Brose et al. 2008; Vucic-Pestic et al. 2010) **and (ii) allometric degree distributions (i.e. the number of predator and prey interactions)(Otto et al. 2007). Our theoretical analyses are supported by empirical data from the most highly resolved, quantitative food web published to date: that of Broadstone Stream (Woodward & Hildrew 2002a; Woodward et al. 2005). While all predators are part of at least one omnivory motif in this food web, their interaction strengths are constrained by their body masses, which allow highly stable motif configurations. Thus, allometry causes a significant deviation from random null models by systematically balancing weak and strong interactions. This solution of the omnivory conundrum explains the prevalence of these motifs in natural food webs.**

Body mass is one of the main characteristics underlying food-web structure (Fig. 3.4.1a) (Woodward et al. 2005; Petchey et al. 2008), determining which coexisting species an organism can attack, handle and consume (Brose; Elton 1926). In foraging ecology, a well documented pattern shows that the ingestion rate of predators depends on their body mass relative to that of their prey (Brose; Elton 1926). More precisely, the relationship between the

per capita ingestion rates of predators and the predator-prey body-mass ratios, *R*, is hump shaped (Fig. 3.4.1b) (Wahlström et al. 2000; Aljetlawi et al. 2004; Vonesh & Bolker 2005; Brose et al. 2008; Vucic-Pestic et al. 2010). This implies that interaction strengths are strong at intermediate body-mass ratios, but weak at either extreme (Wahlström et al. 2000; Aljetlawi et al. 2004; Vonesh & Bolker 2005; Brose et al. 2008; Vucic-Pestic et al. 2010) (Fig. 3.4.1b). This non-linear mass-dependency is usually not taken into account when exploring the stability of food-web motifs. Here, we derived a new multi-prey functional response (i.e., a model relating predator per capita ingestion to the densities of several prey) including this hump-shaped pattern, which is caused by an exponentially increasing prey-specific half saturation density (as shown in the Supplementary Information). We used laboratory data to parametrize this model (see Supplementary Information for a detailed description). In contrast to prior studies, the interaction strengths are constrained by predator and prey body masses (McCann & Hastings 1997; Holt & Polis 1997; McCann et al. 1998; Vandermeer 2006).

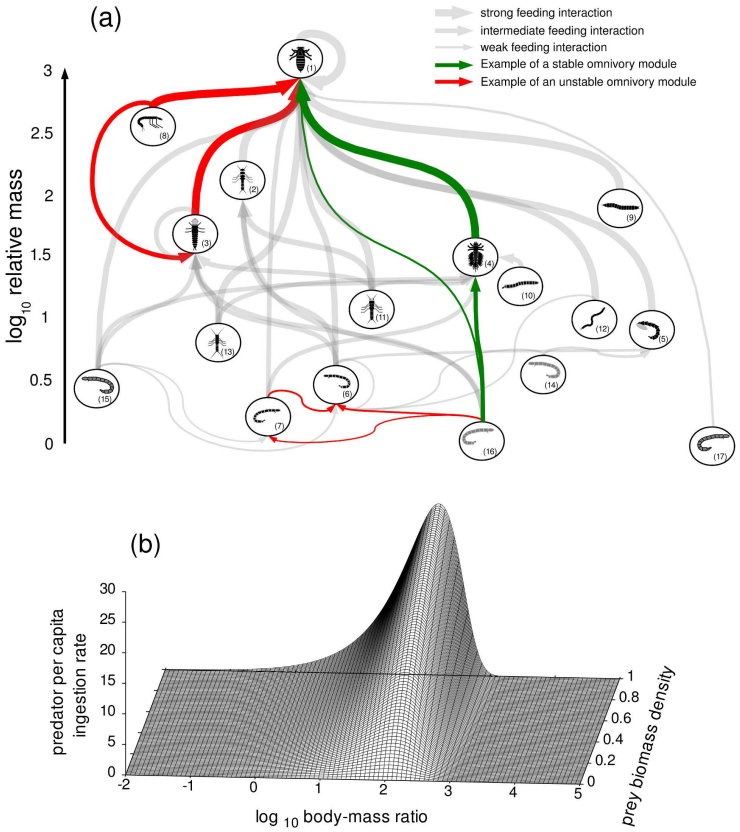

Figure 3.4.1: The allometric structure of natural food webs. (a) The quantitative food web of Broadstone Stream in April, 1997 (Woodward & Hildrew 2002a; Woodward et al. 2005): all species are ordered on the y-axis according to their body-mass ratio relative to the smallest basal species (no. 17, the species *Brillia modesta* (Meigen)). The thickness of the lines shows the strength of the feeding interactions (maximum interaction strength, eqn (12) (McCann et al. 1998), calculated based on empirical gut content data (Woodward & Hildrew 2002a). **(b)** Per capita ingestion rates of predators (functional responses) as a function of the prey biomass density and the predator-prey body-mass ratio, *R*.

We studied the implications of such allometric functional responses for omnivory stability using small motifs whose population dynamics were simulated using a bioenergetic model (Yodzis & Innes 1992; McCann & Hastings 1997; McCann et al. 1998; Otto et al. 2007). For these motifs, we calculated the relative interaction strength (IS_{rel}) as the ratio between the maximum interaction strength (*IS*)(McCann et al. 1998) of the top-basal link and the average

of the other links in the food chain (top-intermediate and intermediate-basal, see Methods and McCann et al. 1998 for details). This shows whether the omnivorous top-basal link is weaker ($IS_{rel} < 1$) or stronger ($IS_{rel} > 1$) than the average interaction strength in the food chain. In our motifs, assuming hump-shaped ingestion rates (Fig. 3.4.1b) means that relative interaction strengths will also follow a hump shaped response to the body-mass ratio between top and basal species (hereafter R_{TB}; Fig. 3.4.2a, see Methods for details). With respect to the Broadstone Stream food web, this implies that small species have generally weak *IS*, whereas large species have strong *IS* (Fig. 3.4.1a, species 6 feeding on species 7 vs. species 1 feeding on species 8). However, if the body-mass ratio of the predators to their prey is high, the resulting *IS* is weak (Fig.3.4.1a, e.g. species 1 feeding on species 16). Furthermore, because of the body-mass dependence of the functional response, the weight factors (McCann & Hastings 1997) (i.e., the proportion of the time that a predator spends foraging on a specific prey) are not free model parameters as in previous studies (McCann & Hastings 1997; McCann et al. 1998), and we show that they follow a negative sigmoid function with predator prey body-mass ratios (Fig. 3.4.2b, see Supplementary Information for details).

Hence, the body-mass dependence of the functional response parameters yields a specific

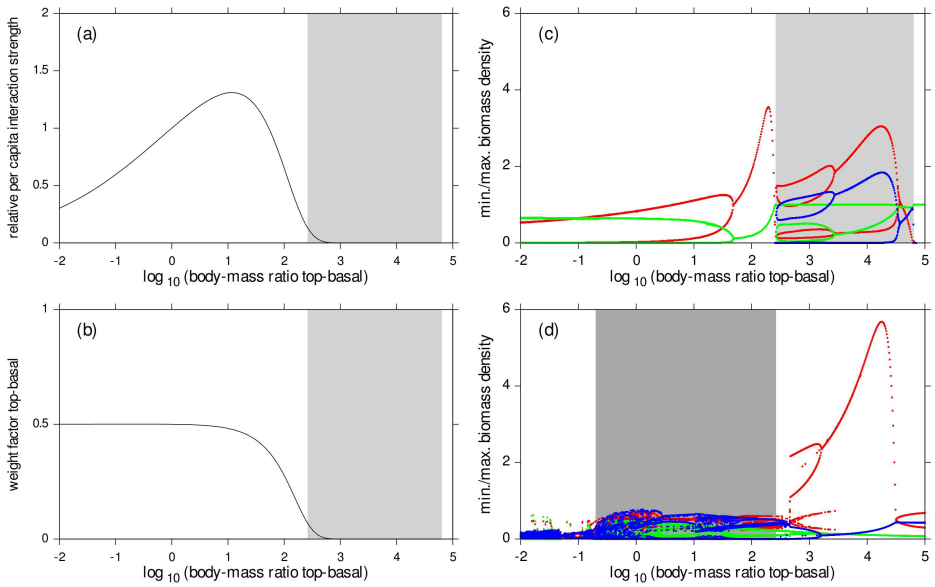

Figure 3.4.2: Consequences of the allometric food-web structures. (a) The per capita relative interaction strength, IS_{rel} (y-axis), follows a hump shaped curve with increasing top-basal body-mass ratio, $\log_{10}(R_{TB})$ (x-axis). **(b)** Weight factor of the interaction between top and basal species, Ω_{TB} (y-axis), depending on their body-mass ratio, $\log_{10}(R_{TB})$ (x-axis); The bifurcation diagrams **(c, d)** show the minima and maxima of population densities of the basal species (green), the intermediate species (blue) and the top species (red) depending on the top-basal body-mass ratio, $\log_{10}(R_{TB})$ (x-axis). Plot **(c)** contains the results of the isolated omnivory motif, examining its intrinsical stability, whereas in plot **(d)** the top species and the intermediate species have additional predators and prey assigned by their allometric degree distributions (mass-dependent generality and vulnerability, see methods for detail). Note that the top-intermediate and intermediate-basal body-mass ratios are half the top-basal body-mass ratio ($R_{TI,IB} = R_{TB} / 2$). The light grey areas show where the system is intrinsically stable, whereas the dark grey area shows the body-mass ratios where the system is extrinsically stable.

distribution of interaction strengths in which the weight factor and the relative interaction strength are simultaneously small when the top predator is sufficiently larger than the basal species (Fig. 3.4.2a,b). Under these conditions, the top-basal link is weak, and based on previous theoretical studies (McCann & Hastings 1997; Holt & Polis 1997; McCann et al. 1998) we expect the omnivory motifs to be persistent.

To test this expectation, we investigated the conditions where omnivory motifs are intrinsically persistent (Kondoh 2008). Consistent with our hypothesis, we found that such motifs are restricted to top-basal body-mass ratios larger than $10^{2.4}$ (Fig. 3.4.2c, light-grey area). Interestingly, these results offer a testable explanation for the stabilizing distribution of interaction strength across omnivory motifs, as opposed to assuming it a priori.

Natural food webs comprise numerous omnivory motifs, including many with low top-basal body-mass ratios which are not expected to be intrinsically stable (see Fig. 3.4.1a, red arrows for an example). But in complex food webs, motifs are embedded within a network of additional interactions with other species, which may yield extrinsically persistent omnivory motifs (Kondoh 2008). For instance, natural food webs exhibit allometric degree distributions meaning that generality (i.e., the number of prey) increases with body mass and vulnerability (i.e., the number of predators) decreases with body mass (Otto et al. 2007). To investigate how the stability of omnivory is affected when embedded within a network compared to an isolated motif, we mimicked the surrounding network by using allometric degree distributions to define the number of additional predator and prey species attached to the omnivory motif (see Methods). Importantly, when taking this surrounding food-web environment into account, omnivorous motifs persist at much lower body-mass ratios than when the motifs are isolated ($\log_{10}(R) > -0.7$, Fig. 3.4.2d, dark-grey area). This extrinsic persistence is caused by the high vulnerability and low generality of the top predator within motifs of low R when placed in the context of the entire food web, which dampens its numerical response and population-level interaction strength.

In agreement with previous studies, we found that low interaction strengths of the top-basal omnivorous link yielded persistent omnivory motifs (intrinsic stability) (McCann & Hastings 1997; Holt & Polis 1997; McCann et al. 1998). Furthermore, the instability at lower R_{TB} ($R_{TB} < 10^{2.4}$) can be overcome by including surrounding species according to empirical allometric degree distributions, which conferred extrinsic stability upon the omnivory motif. Together, our analyses demonstrate that three conditions may cause persistence of omnivory motifs in natural food webs: (1) R_{TB}, should be higher than the body-mass ratios of the food chain, $R_{TI,IB}$; (2) a significant fit of the allometric multi-prey functional response with a hump-shaped relationship between per capita ingestion rates and body-mass ratios, expressed by an exponentially increasing prey-specific half saturation density; and (3) the generality and vulnerability of the predators should increase and decrease, respectively, with increasing body

mass.

These conditions are testable against empirical data. We explored the pattern of interaction strengths and the surrounding food-web structure of the omnivory motifs in the Broadstone Stream food web (Woodward & Hildrew 2002a; Woodward et al. 2005) which is arguably the most highly resolved quantitative food web published to date. Across all omnivory motifs, we found that R_{TB} is systematically higher than $R_{TI,IB}$, consistent with the first condition (Fig. 3.4.3a, *TB* vs. *IB* and *TI*). Subsequently, we used gut-content data of per capita ingestion rates, body masses and prey biomass densities (Woodward & Hildrew 2002a) to fit an allometric multi-prey functional response model to a training data set of the five most common predators and four most common prey species (see Methods for details). Consistent with the second condition, these fitted multi-prey functional responses exhibited a highly significant exponentially increasing prey-specific half saturation density (h_0 = 87.59, p<0.05; ε = 0.00432, p < 0.001) with the body-mass ratio and a power-law relationship between the maximum ingestion rate and the body mass of the predator (c_0 = 0.076, p < 0.001; b =

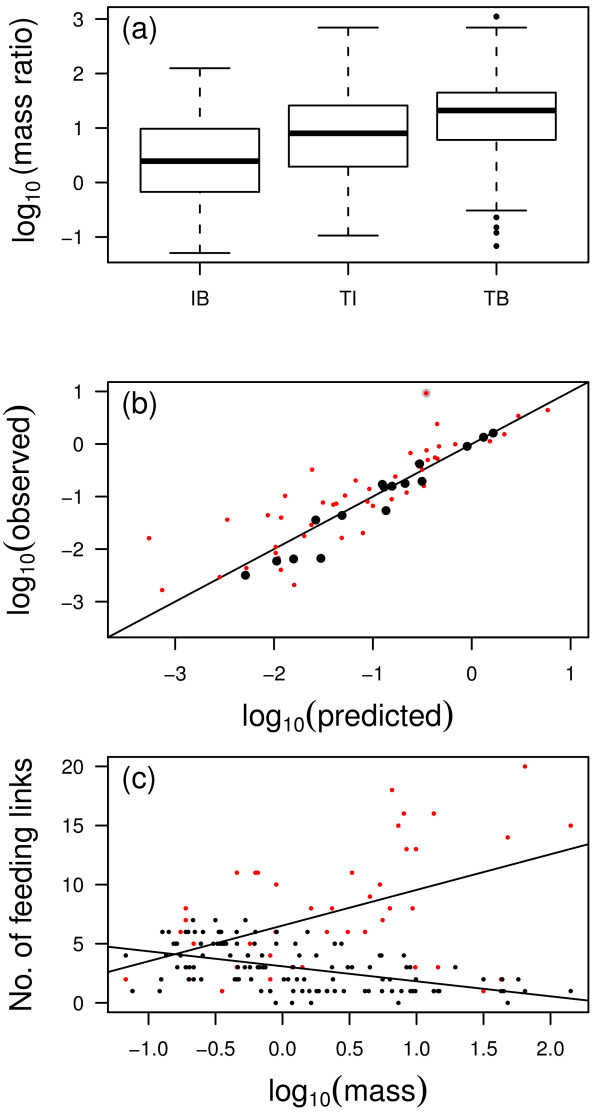

Figure 3.4.3: Empirical analyses of the Broadstone Stream food web. (a) Boxplot of the body-mass ratios, *R*, of the intermediate-basal (*IB*), the top-intermediate (*TI*) and the top-basal links (*TB*). **(b)** Plot of the goodness of the fit of the theoretically derived allometric multi-prey functional response (see Methods, eqn. (15)) to the Broadstone Stream gut content data (observed vs. predicted per capita ingestion rates). The black dots display the training data set (four prey species) and the red dots display the test data set. An outlier is marked with a grey halo. **(c)** Allometric degree distributions: the generality and vulnerability of species in "Broadstone Stream" (Woodward & Hildrew 2002a; Woodward et al. 2005) depending on the body mass of the species, log10(*m*). The generality increases (g = 3.02 $\log_{10}(m)$ + 6.53, p< 0.001, r^2 =0.24), whereas the vulnerability decreases (v = -1.27 $\log_{10}(m)$ + 3.09, p< 0.001, r^2 =0.25) with body mass.

0.91, $p < 0.001$; $r^2 = 0.99$) (see Fig. 3.4.3b black dots, for a goodness of fit graph). To verify if the fit to the data for only four selected prey species is representative of the whole food web, we predicted the ingestion rates in a test data set containing all prey species in the multi-prey functional response model. This yielded an explained variance of 79% after elimination of one outlier (Fig. 3.4.3b, red dots; the outlier has a grey halo). This implies that the prey-specific weight factors follow a sigmoidal decrease with the top-basal body-mass ratios and that the relative interaction strengths follow a hump shaped curve, consistent with the second persistence condition. Moreover, our analyses demonstrated that generality and vulnerability increase and decrease, respectively, with predator body mass (Fig. 3.4.3c), which supports the third persistence condition. As an illustration, the largest species of the Broadstone Stream food web (Woodward & Hildrew 2002a; Woodward et al. 2005), *Cordulegaster boltonii* (species 1, Fig. 3.4.1a), has 16 prey and no predator, whereas smaller predators such as *Trissopelopia longimana* (species 6, Fig. 3.4.1a) have fewer prey but are consumed by several larger predators.

Altogether, our theoretical and empirical results demonstrate that body-mass constraints on interaction-strength parameters and on food web structure yield persistent omnivory motifs. In agreement with prior analyses (McCann & Hastings 1997; McCann et al. 1998; Emmerson & Yearsley 2004), we found that these intrinsic and extrinsic factors create a top-basal link that is weak relative to the top-intermediate and intermediate-basal links. While any interaction strength distribution is possible under random parameter distribution (Holt & Polis 1997; Vandermeer 2006), our analyses show that taking body-mass constraints into account necessarily results in a specific pattern of weak and strong interactions that maintain the persistence of omnivory motifs. Since similar results apply to simple food chains (Otto et al. 2007), our results suggest that body-mass distributions across species in complex (i.e., real) food webs might be a so-far unknown structuring force behind the “balance of nature” and an important mechanism favouring the maintenance of species diversity.

a) Methods

The population model

The stability analyses use a bioenergetic, allometric model that is consistent with prior studies (Yodzis & Innes 1992; Otto et al. 2007). We specifically tailored this model to analyse biomass densities, N, in omnivory motifs with a basal, B, an intermediate, I, and a top predator species, T, embedded in a food-web environment comprising alternative prey, $\beta_{T,I}$, and alternative predators, $\rho_{T,I}$:

$$\frac{dN_B}{dt} = G_B N_B - \frac{F_{IB} N_I}{e} - \frac{F_{TB} N_T}{e} \quad (3.4.1a),$$

$$\frac{dN_I}{dt} = F_{IB} N_B + g_I F_{I\beta_I} N_I - \frac{F_{TI} N_T}{e} - \frac{v_I F_{\rho_I I} N_{\rho_I}}{e} - x_I N_I \quad (3.4.1b),$$

$$\frac{dN_T}{dt} = F_{TB} N_T + F_{TI} N_T + g_T F_{T\beta_T} N_T - \frac{v_T F_{\rho_T T} N_{\rho_T}}{e} - x_T N_T \quad (3.4.1c),$$

where G_B is the logistic growth rate of the basal species, F_{ij} is the functional response of predator i on prey j, e is the assimilation efficiency, g_i and v_i are the number of alternative prey and predators of i, respectively, and x_i is the relative metabolism. The biomass densities of the top and intermediate predators' alternative prey, $\beta_{T,I}$, and alternative predators, $\rho_{T,I}$, follow:

$$\frac{d N_\beta}{dt} = g_j \left[G_\beta N_\beta - \frac{F_{j\beta}}{e} \right] \quad (3.4.1d),$$

$$\frac{d N_\rho}{dt} = v_j \left[F_{\rho j} N_\rho - x_\rho N_\rho \right] \quad (3.4.1e).$$

The logistic growth G_i of species i is described by

$$G_i = r_i \left(1 - \frac{B_i}{K_i}\right) \quad (3.4.2),$$

where r_i is the relative intrinsic growth rate and K_i is the normalized carrying capacity (see below). The functional response follows:

$$F_{ij} = \frac{x_i y_i \Omega_{ij} N_j}{\Phi_{tot} + \sum \Omega_{ik} N_k} \quad (3.4.3)$$

where x_i is the relative metabolism and y_i is the relative ingestion constant; Φ_{tot} is the relative total half saturation density and Ω_{ik} is a weight factor (see below and Supplementary Information for details).

Consistent with prior studies, the per unit biomass rates of metabolism, biomass growth (W_i) and maximum ingestion (c_{max}) decrease with a -¼ power law with the species body mass (Peters 1983; Yodzis & Innes 1992; Brown et al. 2004; Savage, Gillooly, Brown, et al. 2004):

$$\frac{X_i}{m_i} = a_X m_i^{-0.25} \quad (3.4.4a),$$

$$\frac{W_i}{m_i} = a_W m_i^{-0.25} \quad (3.4.4b),$$

$$\frac{c_{max}}{m_i} = a_c m_i^{-0.25} \quad (3.4.4c),$$

where m_i is body mass and $a_{X,W,C}$ are allometric constants. In line with prior approach (Yodzis & Innes 1992), we define the time scale of the system and generalize analyses across body-mass scales by normalizing the growth and respiration rates by the growth rate of the first basal species (yielding $r_B = 1$):

$$r_i = \frac{W_i}{W_B} = \frac{a_W}{a_W} \frac{m_i^{-0.25}}{m_B^{-0.25}} = R_{iB}^{-0.25} \quad (3.4.5a);$$

$$x_i = \frac{X_i}{m_i W_B} = \frac{a_X}{a_W} \frac{m_i^{-0.25}}{m_B^{-0.25}} = x_0 R_{iB}^{-0.25} \quad (3.4.5b),$$

where R_{iB} is the body mass ratio of the target species to the basal species. Subsequently, the maximum ingestion rates are normalized by the respiration rates:

$$y_i = \frac{c_{max}}{X_i} = \frac{a_c}{a_X} \quad (3.4.5c).$$

As any biomass density, the carrying capacities follow quarter power-law relationships with body masses (Peters 1983; Meehan 2006a):

$$k_i = k_0 m_i^{0.25} \quad (3.4.6a),$$

To avoid effects of basal species richness on system enrichment (see Rall et al. (2008) and references therein for a detailed description of enrichment effects), we set the systems carrying capacity to unity and calculated the relative carrying capacity of each basal species K_i as

$$K_i = \frac{k_i}{\sum_{j=1}^{j=n} k_j} \quad (3.4.6b),$$

where the sum of all carrying capacities k_j is constant.

Prior studies used constant half saturation densities of the functional responses that are independent of the species' body masses (Yodzis & Innes 1992; McCann & Hastings 1997; McCann et al. 1998; Otto et al. 2007). Our theoretical derivations show that the frequently documented hump-shaped relationships between attack rates and predator-prey body-mass

ratios (Wahlström et al. 2000; Aljetlawi et al. 2004; Vonesh & Bolker 2005; Brose et al. 2008; Vucic-Pestic et al. 2010) imply prey-specific half saturation densities following exponential relationships with predator-prey body-mass ratios (see Supplementary Information for details):

$$h_{ij} = h_0 e^{(\varepsilon R_{ij})} \quad (3.4.7a),$$

where h_0 is an allometric constant and ε determines the shape of the exponential curve and R_{ij} is the body mass ratio of a predator to its prey. Subsequently, the prey-specific half saturation density, h_{ij}, is normalized by the total carrying capacity yielding:

$$\eta_{ij} = \frac{h_{ij}}{\sum_{j=1}^{j=n} k_j} = \frac{h_0}{\sum_{j=1}^{j=n} k_j} e^{\varepsilon R_{ij}} = \eta_0 e^{\varepsilon R_{ij}} \quad (3.4.7b),$$

where η_0 is an allometric constant when the sum of k_j is a constant (Yodzis & Innes 1992). In two-prey functional response models, the weight factor and the relative total half saturation density are calculated by

$$\Omega_{ij} = \frac{\eta_{ik}}{(\eta_{ij} + \eta_{ik})} \quad (3.4.8),$$

and

$$\Phi_{tot} = \frac{\eta_{ij}\eta_{ik}}{(\eta_{ij} + \eta_{ik})} \quad (3.4.9),$$

respectively; but see the supplement for a detailed derivation of the functional response and its parameters, as well as for more complex total half saturation densities containing more than two prey species.

In our analyses, the surrounding food-web structure of the omnivory motif was included as the number of alternative predators, v_i, and alternative prey, g_i, of the top and intermediate species, which depend closely on their vulnerability and generality. Allometric degree distributions of these species' characteristics (Otto et al. 2007) allow calculating v_i and g_i as:

$$v_i = v_0 \log_{10}(R_{iB}) + L_0 - L_i \quad (3.4.10a)$$

$$g_i = g_0 \log_{10}(R_{iB}) + L_0 - L_i \quad (3.4.10b)$$

where v_0 and g_0 are allometric constants, L_0 is a system-specific normalisation constant determining the number of prey and predators of a species of equivalent size to the basal species and L_i is the number of interactions to the other species in the omnivory motif. Note that the minimum population density of the alternative predators and alternative prey are set to

(k_i^{-6}) to ensure that the surrounding food web is persistent.

Parameter space

We used empirically derived constants to parametrize our model (Brown et al. 2004; Otto et al. 2007). The metabolic constant x_0 is 0.2227, y is 8 (Otto et al. 2007). The half saturation parameters ε and η_0 are 0.01064 and 0.47, respectively, which equates to an optimal foraging body mass ratio of approximately 50 (Brose et al. 2008), and yielding a prey specific half saturation term of 0.5 as used in a previous study (Otto et al. 2007) at this optimal body mass ratio. The structural constants g_0 and v_0 are 1.5 and -0.75, respectively (Otto et al. 2007). If v_i and g_i have negative values, they are set to zero.

Calculation of the relative interaction strength

McCann et al. (1998) introduced a method to calculate the maximum interaction strength of a predator upon its prey. The per capita interaction strength or predation possibility by a predator i on a prey j is defined as

$$\alpha_{ij} = \frac{F_{ij}}{N_j} \tag{3.4.11}$$

In consequence the interaction strength should be the highest when the biomass density, N_j, of species j approaches zero. This yields a maximum interaction strength ($N_j \rightarrow 0$) of

$$IS_{ij} = \frac{c_{max}\,\Omega_{ij}}{H_{tot}} \tag{3.4.12}$$

Previous studies suggested that the ratio between the interaction strength of the omnivorous interaction to the other interactions in the food chain determine the stability of the system (McCann & Hastings 1997; Holt & Polis 1997; McCann et al. 1998). When the omnivorous link becomes weak relative to the other links (the omnivory motif becomes more “chain-like”), the system should be stabilised (Holt & Polis 1997; McCann et al. 1998). Following prior studies(McCann et al. 1998), we calculated this ratio or relative interaction strength IS_{rel} by

$$IS_{rel} = \frac{2\,IS_{TB}}{IS_{TI} + IS_{IB}} \tag{3.4.13}.$$

Functional response fitting to gut content data. For fitting the multi-prey functional response model to the empirical gut content data from Broadstone Stream (Woodward & Hildrew 2002a; Woodward et al. 2005), we split the empirical data into a training and a test data set.

The training data set contains five predators (*Cordulegaster boltonii* (Donovan); *Macropelopia nebulosa* (Meigen); *Plectrocnemia conspersa* (Curtis); *Sialis fuliginosa* (Pictet); *Trissopelopia longimana* (Staeger)) and four prey species (*Heterotrissocladius marcidus* (Walker); *Nemurella pictetii* (Klapalek); *Trissopelopia longimana* (Staeger); *Zavrelimyia barbatipes* (Kieffer)) that were present and eaten at every sampling date by all five predators. To ensure that the estimated values do not vary between prey specific functional responses, we fitted the model against the summed feeding rates. The model (supplementary Eqn. 3.4.21e) becomes:

$$F_{i\sum k} = \frac{\sum_{k=1}^{k=n} c_{max}\,\Omega_{ik}\,N_k}{H_{tot} + \sum_{k=1}^{k=n} \Omega_{ik}\,N_k} \qquad (3.4.14).$$

Inserting the allometric dependencies (supplementary Eqn. 3.4.17 and 3.4.19) into equation (3.4.14) and simplifying it for the case of four prey species (following supplementary Eqn. 3.4.23a and 3.4.23b) yields:

$$F_{i\sum k} = \frac{((c_0 m^a N_1 e^{(\varepsilon R_{i2})} + c_0 m^a N_2 e^{(\varepsilon R_{i1})}) e^{(\varepsilon R_{i3})} + c_0 m^a N_3 e^{(\varepsilon R_{i2} + \varepsilon N_{i1})}) e^{(\varepsilon R_{i4})} + c_0 m^a N_4 e^{(\varepsilon R_{i3} + \varepsilon R_{i2} + \varepsilon R_{i1})}}{(((h_0 e^{(\varepsilon R_{i1})} + N_1) e^{(\varepsilon R_{i2})} + N_2 e^{(\varepsilon R_{i1})}) e^{(\varepsilon R_{i3})} + N_3 e^{(\varepsilon R_{i2} + \varepsilon R_{i1})}) e^{(\varepsilon R_{i4})} + N_4 e^{(\varepsilon R_{i3} + \varepsilon R_{i2} + \varepsilon R_{i1})}} \qquad (3.4.15).$$

We used non-linear least squares regressions to fit this model to the training data set containing the empirical biomass densities, N [mg m^{-2}], body masses, m [mg], and per capita feeding rates $F_{i\Sigma k}$ [mg day^{-1}] (gut contents). The model parameters (c_0, a, ε, h_0) estimated for the training data set were subsequently used to predict the per capita ingestion rates of the test data set containing the entire Broadstone Stream food web with all species and their interactions.

b) Supplementary Information

Derivation of the functional response model. A functional response describes the feeding F_{ij} of a predator i on a prey j in dependence on the prey biomass density N_j and follows:

$$F_{ij} = \frac{a_{ij} N_j}{1 + a_{ij} T_h N_j} \qquad (3.4.16a),$$

where a_{ij} is the attack rate [m²/day] (also known as: instantaneous search or capture rate) and T_h is the handling time [days/g], the time a predator needs to subdue, ingest and digest a prey biomass unit. Instead of this mechanistic description of a functional response, most theoretical studies use a model considering a maximum ingestion rate, c_{ij}, and a half saturation density, h. The maximum ingestion rate is defined as the inverse of the handling time ($T_h = 1/c_{ij}$). The

handling time is replaced by 1 over c_{ij} yielding

$$F_{ij} = \frac{a_{ij} N_j}{1 + a_{ij} \frac{1}{c_{ij}} N_j} \quad (3.4.16b).$$

Subsequently, the right side of the equation is multiplied by c_{ij} (Eqn. 3.4.16c).

$$F_{ij} = \frac{c_{ij} a_{ij} N_j}{c_{ij} + a_{ij} N_j} \quad (3.4.16c),$$

Dividing the right side of equation (3.4.16c) by the attack rate leads to a formulation of c_{ij} over a_{ij}:

$$F_{ij} = \frac{c_{ij} N_j}{\frac{c_{ij}}{a_{ij}} + N_j} \quad (3.4.16d),$$

that can be replaced by the term of the half saturation density:

$$F_{ij} = \frac{c_{ij} N_j}{h_{ij} + N_j} \quad (3.4.16e).$$

The body mass dependency of c_{ij} is well documented in several studies (Brown et al. 2004; Vucic-Pestic et al. 2010) and follows a 3/4 power law, as is the case for many other biological rates;

$$c_{ij} = c_0 m_i^b \quad (3.4.17),$$

where c_0 is a constant and b is the allometric slope of the power law. Also, the attack rate should follow a power law relationship according to increased travel speed and increasing home range size with increasing body mass of the predator (Peters 1983). However, most recent foraging studies showed that the attack rate decreases after reaching an optimal body mass ratio to its prey (Wahlström et al. 2000; Aljetlawi et al. 2004; Vonesh & Bolker 2005; Brose et al. 2008; Vucic-Pestic et al. 2010). This decrease is usually described by an exponential decrease of the attack rates in dependence on the body mass ratio of a predator to its prey:

$$a_{ij} \approx a_0 m_i^b e^{-(\varepsilon \frac{m_i}{m_j})} \quad (3.4.18).$$

The attack rates are described by a constant a_0, an allometric power law with an exponent of b, and an exponential decrease with the body mass ratio of the predator to its prey and a shaping

parameter, ε, defining the steepness of the exponential curve.

Subsequently, the half saturation density can be calculated by dividing equation (3.4.17) by equation (3.4.18):

$$h_{ij} = \frac{c_0 m^b}{a_0 m_i^b e^{-(\varepsilon \frac{m_i}{m_j})}} \quad (3.4.19a),$$

$$h_{ij} = \frac{c_0}{a_0} \exp(\varepsilon \frac{m_i}{m_j}) \quad (3.4.19b),$$

$$h_{ij} = h_0 \exp(\varepsilon \frac{m_i}{m_j}) \quad (3.4.19c),$$

where $h_0 = c_0 / a_0$.

However, food webs comprise multiple prey for predators. The multi-species formulation of a mechanistic functional response is (Murdoch & Oaten 1975; Koen-Alonso 2007),

$$F_{ij} = \frac{a_{ij} B_{ij}}{1 + \sum a_{ik} Th_{ik} B_{ik}} \quad (3.4.20),$$

where the parameters are the same as in equation (3.4.16) except for extra terms for the attack rates, handling times and biomass densities of alternative prey species, a_{ik}, Th_{ik} and B_{ik}, respectively. To convert the multi-prey functional response into a form containing half saturation rates and maximum ingestion rates as for the prey-specific functional response (Eqn. (3.4.16) to Eqn. (3.4.19)) requires two assumptions: (1) the handling time per unit biomass is equal for all prey species and equals the inverse of the maximum ingestion rate, c_{max} (Koen-Alonso 2007), and (2) the prey-specific attack rate can be summed to a total attack rate ($a_T = \Sigma a_{ik}$) implying that the prey-specific attack rate is a fraction of the total attack rate ($a_{ik} = \Omega_{ik}\ a_T$) (Koen-Alonso 2007). This fraction of the total attack rate is described by the weight factor, Ω_{ik}, where the sum of all weight factors yields unity. Rewriting equation (3.4.20) yields

$$F_{ij} = \frac{a_{ij} B_j}{1 + \frac{1}{c_{max}} \sum a_{ik} B_k} \quad (3.4.21a);$$

$$F_{ij} = \frac{c_{max} a_{ij} B_j}{c_{max} + \sum a_{ik} B_k} \quad (3.4.21b);$$

$$F_{ij} = \frac{c_{max}\,\Omega_{ij}\,a_T\,B_j}{c_{max} + a_T \sum \Omega_{ik} B_k} \quad (3.4.21c);$$

$$F_{ij} = \frac{c_{max}\,\Omega_{ij}\,B_j}{\frac{c_{max}}{a_T} + \sum \Omega_{ik} B_k} \quad (3.4.21d);$$

$$F_{ij} = \frac{c_{max}\,\Omega_{ij}\,B_j}{H_T + \sum \Omega_{ik} B_k} \quad (3.4.21e).$$

In equation (3.4.21d) to equation (3.4.21e), the term c_{max} / a_T is replaced by the total half saturation rate H_T. This multi-prey functional response is generally used for modelling multi-species population dynamics (Williams & Martinez 2004a; Brose et al. 2005b; Brose et al. 2006b; Rall et al. 2008; Brose 2008). However, empirical studies generally study simple one-predator one-prey functional responses (prey-specific functional responses, equations (3.4.16)-(3.4.19)). The maximum ingestion rate c_{max} is the same in both functional response models, because it is constant across all prey species (Koen-Alonso 2007). The weight factors and the total half saturation density are calculated based on the maximum ingestion rate and the prey-specific half saturation densities:

$$\Omega_{ik} = \frac{a_{ij}}{a_T} = \frac{(c_{max}/h_{ij})}{(\sum c_{max}/h_{ik})} \quad (3.4.22a);$$

$$H_T = \frac{c_{max}}{a_T} = \frac{c_{max}}{(\sum c_{max}/h_{ik})} \quad (3.4.22b).$$

As an example, with two prey species the equations (3.4.22a) and (3.4.22b) can be simplified to

$$\Omega_{ij} = \frac{h_{ik}}{(h_{ij} + h_{ik})} \quad (3.4.23a)$$

$$H_T = \frac{h_{ij}\,h_{ik}}{(h_{ij} + h_{ik})} \quad (3.4.23b).$$

With an increasing number of prey species, the simplified equations always contain only the different prey specific half saturation densities (data not shown). Based on equation (3.4.19), it follows that both, the total half saturation density and the weight factors, depend only on the predator-prey body-mass ratio. In the case of omnivory motifs, where the top-basal body-mass ratio is double the body mass ratios in the food chain, this yields a sigmoid decrease in the weight factor with increasing body-mass ratio.